The Plant Cell, Vol. 26: 2249–2264, May 2014, www.plantcell.org

OPT3 Is a Phloem-Specific Iron Transporter That Is Essential for Systemic Iron Signaling and Redistribution of Iron and Cadmium in *Arabidopsis*[W][OPEN]

Zhiyang Zhai,[a,1] Sheena R. Gayomba,[a,1] Ha-il Jung,[a,1] Nanditha K. Vimalakumari,[a,1] Miguel Piñeros,[b,1] Eric Craft,[b] Michael A. Rutzke,[a,b] John Danku,[c] Brett Lahner,[d] Tracy Punshon,[e] Mary Lou Guerinot,[e] David E. Salt,[c] Leon V. Kochian,[b] and Olena K. Vatamaniuk[a,2]

[a] Department of Crop and Soil Sciences, Cornell University, Ithaca, New York 14853
[b] Robert W. Holley Center for Agriculture and Health, U.S. Department of Agriculture–Agricultural Research Service, Ithaca, New York 14853
[c] Institute of Biological and Environmental Sciences, University of Aberdeen, AS24 3UU Scotland, United Kingdom
[d] Center for Plant Environmental Stress Physiology, Purdue University, West Lafayette, Indiana 47907
[e] Department of Biological Sciences, Dartmouth College, Hanover, New Hampshire 03755

Iron is essential for both plant growth and human health and nutrition. Knowledge of the signaling mechanisms that communicate iron demand from shoots to roots to regulate iron uptake as well as the transport systems mediating iron partitioning into edible plant tissues is critical for the development of crop biofortification strategies. Here, we report that OPT3, previously classified as an oligopeptide transporter, is a plasma membrane transporter capable of transporting transition ions in vitro. Studies in *Arabidopsis thaliana* show that OPT3 loads iron into the phloem, facilitates iron recirculation from the xylem to the phloem, and regulates both shoot-to-root iron signaling and iron redistribution from mature to developing tissues. We also uncovered an aspect of crosstalk between iron homeostasis and cadmium partitioning that is mediated by OPT3. Together, these discoveries provide promising avenues for targeted strategies directed at increasing iron while decreasing cadmium density in the edible portions of crops and improving agricultural productivity in iron deficient soils.

INTRODUCTION

Iron (Fe) is essential for plant growth and development and is an important component of the human diet. Cadmium (Cd), on the other hand, is a nonessential and highly toxic element that competes with Fe for uptake and partitioning in plant tissues, thus posing a threat to crop productivity and human health. The ability of Fe to change its oxidation state ($Fe^{3+} \leftrightarrow Fe^{2+}$) highlights its importance in biological processes that involve electron transfer reactions (e.g., respiration and photosynthesis). However, the same property imposes toxicity when Fe is accumulated in cells in excess due to its ability to promote the formation of reactive oxygen species (Valko et al., 2005). Bioavailability of Fe in aerobic soils with neutral to basic pH is below the limits required to sustain plant growth and development because insoluble Fe(III) chelates prevail under these conditions. Consequently, alkaline soils, occupying ~30% of the world's arable lands, are considered Fe-limiting for plant growth (Marschner, 1995). To increase Fe bioavailability, *Arabidopsis thaliana* and other dicotyledonous and nongraminaceous monocotyledonous plants use a reduction strategy (Hindt and Guerinot, 2012; Kobayashi and Nishizawa, 2012). In brief, this mechanism includes the acidification of the rhizosphere by the H^+-ATPases of the *Arabidopsis* H^+-ATPase family (Santi and Schmidt, 2009), the reduction of Fe(III) chelates to soluble Fe(II) by the root surface-localized ferric chelate reductase FRO2 (Robinson et al., 1999), and the subsequent uptake of Fe(II) into root epidermal cells by the high-affinity Fe(II) transporter IRT1 (Eide et al., 1996). The FRO2/IRT1 system constitutes the major pathway for Fe entry into root epidermal cells. Given the essential and toxic nature of Fe, expression of *FRO2* and *IRT1* is under tight local and long-distance regulation (Hindt and Guerinot, 2012; Kobayashi and Nishizawa, 2012). Interestingly, Fe itself plays a signaling role and is regarded as a positive regulator of local signaling (Vert et al., 2003). In contrast, it is suggested to act as a negative regulator of shoot-to-root signaling via the phloem (Hindt and Guerinot, 2012; Kobayashi and Nishizawa, 2012). However, the latter suggestion has not been substantiated experimentally.

After initial uptake from the soil into root epidermal cells, Fe moves symplastically toward the vasculature and is effluxed into the xylem vessels where it is chelated with citrate to form a tri-Fe(III) tricitrate complex that undergoes long-distance transport to the shoot (Durrett et al., 2007). Another strong Fe ligand that is

[1] These authors contributed equally to this work.
[2] Address correspondence to okv2@cornell.edu.
The author responsible for distribution of materials integral to the findings presented in this article in accordance with the policy described in the Instructions for Authors (www.plantcell.org) is: Olena K. Vatamaniuk (okv2@cornell.edu).
[W] Online version contains Web-only data.
[OPEN] Articles can be viewed online without a subscription.
www.plantcell.org/cgi/doi/10.1105/tpc.114.123737

responsible for the translocation of Fe in the phloem is a nonproteinogenic amino acid, nicotianamine (NA) (Curie et al., 2009). The molecular machinery contributing to root-to-shoot partitioning of Fe, its redistribution between source and sink tissues, and events involved in shoot-to-root communication of shoot Fe status are much less understood. The key identified players in *Arabidopsis* are the multidrug and toxin efflux family member FRD3, the ferroportin (FPN)-like protein FPN1 (alias IREG1 [IRON REGULATED1]), and members of two distinct clades of the Oligopeptide Transporter family, the Yellow Stripe-like (YSL) proteins and the Oligopetide Transporters (OPTs), for which the family was named (Rogers and Guerinot, 2002; Green and Rogers, 2004; Morrissey et al., 2009; Lubkowitz, 2011). FRD3 mediates citrate release into the apoplastic space and is essential for xylem-based Fe movement and Fe nutrition in tissues lacking symplastic connections (Rogers and Guerinot, 2002; Green and Rogers, 2004; Roschzttardtz et al., 2011), FPN1 is proposed to load Fe into the xylem (Morrissey et al., 2009), while YSL2 is suggested to be involved in lateral distribution of Fe-NA complexes from the xylem into neighboring cells (DiDonato et al., 2004; Schaaf et al., 2005).

The phloem-based long-distance transport to sink tissues, such as young leaves, developing seeds, and roots, involves apoplastic loading of Fe into the companion cells/sieve elements complex (CC/SE) as well as unloading into corresponding sink tissues. Knowledge of transporters contributing to phloem loading/unloading is scarce. The main contributors in this process are At-YSL1, At-YSL3, and Os-YSL2, which mediate Fe-NA transport and facilitate Fe loading into seeds of *Arabidopsis* and rice (*Oryza sativa*) (Waters et al., 2006; Chu et al., 2010; Ishimaru et al., 2010). In this regard, a member of the OPT family in *Arabidopsis*, OPT3, has been under scrutiny for more than a decade since the discovery of its role in Fe homeostasis (Stacey et al., 2002, 2006, 2008). Studies in heterologous systems have implicated *Arabidopsis* and rice OPT family members, and the closest OPT3 homolog from *Brassica juncea*, Bj-GT1, in transport of synthetic peptides, as well as of the ubiquitous tripeptide GSH (Bogs et al., 2003; Cagnac et al., 2004; Osawa et al., 2006). However, the physiological substrate(s) of OPTs, including OPT3, has not yet been identified. With respect to Fe homeostasis, it was shown that (1) *OPT3* mRNA is expressed in the vasculature where it is transcriptionally upregulated by Fe deficiency; (2) OPT3 is involved in Fe accumulation in seeds, and loss of this function is suggested to cause embryo lethality in the *opt3-1* null mutant; (3) the *opt3-2* knockdown mutant harboring a T-DNA insertion in the promoter region is viable but accumulates high levels of Fe in both shoots and roots while exhibiting constitutive Fe starvation phenotypes (e.g., upregulated expression of *IRT1* and *FRO2*) even when the mutant is grown under Fe-sufficient conditions (Stacey et al., 2002, 2008). However, the mechanistic basis of the misregulated Fe signaling in the *opt3-2* knockdown mutant and the physiological substrate of OPT3 are unknown.

It is noteworthy that disrupted Fe signaling observed in the *opt3-2* mutant has been also found in several other mutants, such as the *frd3* (*man1*) mutant and the quadruple nicotianamine synthase mutant (*nas4x-1*) of *Arabidopsis*, the *dgl* and *brz* iron homeostasis mutants of pea (*Pisum sativum*), and the *chloronerva* (*chln*) mutant of tomato (*Solanum lycopersicum*), all showing constitutive activation of Fe acquisition genes even when grown under Fe-sufficient conditions (Scholz et al., 1985; Grusak et al., 1990; Kneen et al., 1990; Grusak and Pezeshgi, 1996; Schuler et al., 2012). Importantly, foliar application of Fe blocked the expression of Fe-acquisition genes in the wild-type cultivars and in *frd3-3*, *brz*, and *chln* mutants, but not in *opt3-2* and *dgl* mutants, reinforcing the previous suggestion of the existence of an Fe-related repressive signal moving from leaves to roots and pointing to distinct molecular mechanisms of shoot-to-root communication of Fe status in different mutants (García et al., 2013, Maas et al., 1988). Therefore, the identification of the physiological substrate of OPT3 is among the key questions to be addressed with respect to its role in Fe homeostasis and shoot-to-root Fe signaling.

Iron homeostasis is tightly linked with homeostasis of essential elements such as zinc (Zn), manganese (Mn), cobalt (Co), and the nonessential and potentially toxic element cadmium (Cd) due to the low substrate specificity of IRT1 (Eide et al., 1996; Baxter et al., 2008). The crosstalk between essential elements and Cd has been under scrutiny over past decades because Cd is increasingly released into the environment as industrial and consumer waste and poses a threat to crop productivity and human health (Järup, 2003). Cadmium causes stunting and chlorosis in plants and affects major biochemical processes, including redox balance, photosynthesis, and water status (Hasan et al., 2009). Cadmium is detoxified in the cytosol by forming a bidentate Cd-GS_2 complex with GSH (Li et al., 1997), which then facilitates synthesis of strong Cd ligands, phytochelatins (PC) (Rea 2012). Cd-PC complexes, as well as free Cd ions, are either sequestrated into the vacuole in the root or bypass the vacuole and instead load into xylem vessels of the root to travel into shoot with the transpiration stream and are eventually loaded into vacuoles in the shoot (Salt et al., 1995; Wong and Cobbett, 2009; Park et al., 2012). With respect to Fe nutrition, it has been shown that Cd competes with Fe(II) for the uptake into root epidermal cells via IRT1 and that *IRT1*-overexpressing *Arabidopsis* plants accumulate more Cd (Eide et al., 1996; Connolly et al., 2002). A recent finding that co-overexpression of a master regulator of Fe homeostasis, FIT, with its binding partners, the transcription factor bHLH38 or bHLH39, enhances Cd tolerance in *Arabidopsis* by increasing Cd sequestration in roots and improving Fe homeostasis of shoots (Wu et al., 2012) further emphasizes important relationship between Cd resistance and Fe homeostasis.

Here, we report that a member of the oligopeptide transporter family in *Arabidopsis*, OPT3, is a phloem-specific transporter that mediates Fe loading into the phloem, and, unlike other members of this family, transports transition metal ions rather than small peptides as the name oligopeptide transporter implies. Our findings also suggest that by loading of Fe into the phloem in leaves, OPT3 regulates both signaling of Fe demand from shoots to roots and Fe transport to developing tissues. We also present data showing an aspect of crosstalk between Fe homeostasis and Cd partitioning that is mediated by OPT3.

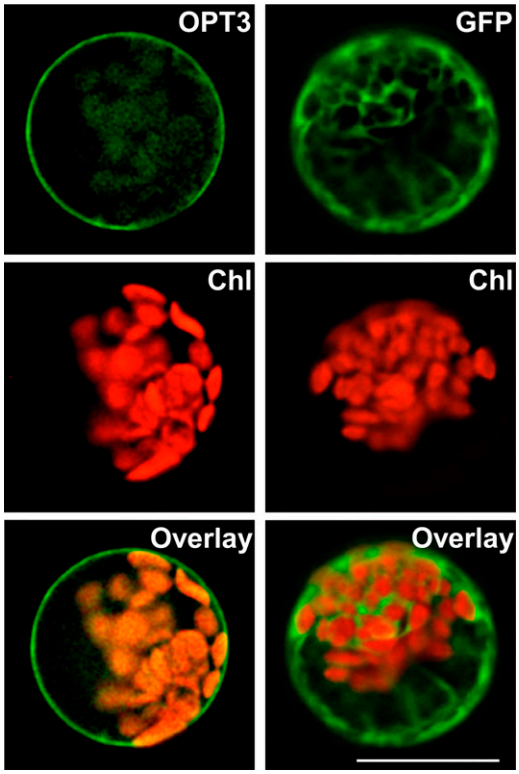

Figure 1. OPT3 Localizes to the Plasma Membrane in *Arabidopsis* Protoplasts.

GFP-mediated fluorescence, derived from the OPT3-GFP (OPT3) constructor or the empty GFP vector (GFP), and chlorophyll autofluorescence (Chl) were visualized using FITC or rhodamine filter sets. Superimposed images of chlorophyll autofluorescence and GFP-mediated fluorescence (Overlay) were created to demonstrate that green fluorescence was derived from GFP. Bar = 20 μm.

RESULTS

OPT3 Localizes to the Plasma Membrane in *Arabidopsis* Protoplasts

To begin the investigation of the role of OPT3 in the regulation of Fe deficiency responses, its physiological substrate and function in *Arabidopsis*, we first determined its subcellular localization. We fused the *OPT3* cDNA with a coding sequence of green fluorescent protein (GFP) and transiently expressed the OPT3-GFP construct under the control of the cauliflower mosaic virus 35S promoter in *Arabidopsis* protoplasts. GFP-mediated fluorescence was present in the cytosol and did not overlap with chlorophyll autofluorescence in protoplasts transfected with GFP only (Figure 1). In contrast, OPT3-GFP–mediated fluorescence was present at the periphery of transfected protoplasts, did not overlap with chlorophyll autofluorescence, and was absent in the tonoplast (Figure 1). The plasma membrane localization of OPT3 was further confirmed by transient expression of the OPT3-GFP construct in onion (*Allium cepa*) epidermal cells (Supplemental Figure 1). Therefore, we concluded that OPT3 localizes to the plasma membrane in *Arabidopsis* and thus is involved in movement of substrate(s) into or out of the cell rather than in subcellular (e.g., vacuolar) sequestration.

OPT3 Does Not Complement the GSH Uptake Deficiency of the *S. cerevisiae* GSH Uptake Mutant, *opt1*, and Does Not Mediate GSH Uptake in Yeast

The closest OPT3 homolog from *B. juncea*, Bj-GT1, transports GSH (Bogs et al., 2003). To test whether OPT3 could transport GSH as well, we used functional complementation and in vitro transport assays in the *S. cerevisiae* mutant lacking a plasma membrane–localized GSH transporter, Opt1p (alias Hgt1p) (Bourbouloux et al., 2000). As *opt1* mutant cells do not grow on medium with GSH as the sole source of sulfur, we first tested whether heterologously expressed At-*OPT3* could complement the GSH uptake deficiency of the *opt1* mutant. We transformed *opt1* mutant cells with the vector expressing Sc-*OPT1* or At-*OPT3* (*opt1*/*OPT1* and *opt1*/*OPT3*, respectively) or with the empty vector (*opt1*/*EV*) and analyzed the ability of transformants to grow in liquid minimal medium with GSH as the only sulfur source. As a control, we replaced GSH with ammonium sulfate. We found that while the growth of *opt1*/*OPT3* and *opt1*/*EV* yeast lines was undistinguishable from *opt1*/*OPT1* in control medium (Supplemental Figure 2), only cells transformed with Sc-*OPT1* were able to grow in medium with GSH as the only source of sulfur (Figure 2A). These data indicated that heterologously expressed At-*OPT3* could not complement the GSH uptake defect of the *opt1* mutant. We also performed in vitro uptake assays and found that while *opt1*/*OPT1* cells absorb [^{35}S]GSH, *opt1*/*OPT3* and *opt1*/*EV* yeast lines were not able to accumulate [^{35}S]GSH (Figure 2B). These data suggested that, in this heterologous system, At-OPT3 does not mediate GSH transport.

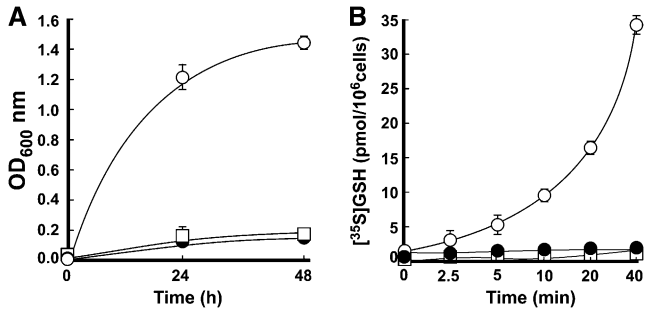

Figure 2. OPT3 Does Not Mediate GSH Transport in *S. cerevisiae*.

(A) *S. cerevisiae opt1* mutant cells expressing Sc-*OPT1*cDNA (open circles), the empty vector (closed circles), or vector with the At-*OPT3* cDNA insert (open squares) were grown in SC-S media supplemented without or with 200 μM GSH. OD values were measured after 24 and 48 h of culturing at 30°C.

(B) Time course of in vitro [^{35}S]GSH uptake by *opt1* mutant cells expressing Sc-*OPT1*cDNA (open circles), the empty vector (closed circles), or vector with the At-*OPT3* cDNA insert (open squares). Error bars represent SE (n = 3).

Heterologously Expressed *OPT3* Partially Rescues the Fe Uptake Defect of the *S. cerevisiae fet3 fet4* Mutant

Because OPT3 has been linked to Fe homeostasis in *Arabidopsis* (Stacey et al., 2002, 2008; Wintz et al., 2003), we next tested whether it would be able to rescue Fe accumulation defects of the *S. cerevisiae fet3 fet4* mutant, which lacks both high- and low-affinity Fe uptake systems and cannot grow in Fe-limited conditions (Dix et al., 1994). DY1457 wild-type and *fet3 fet4* mutant yeast cells were transformed with an empty vector, and the *fet3 fet4* mutant was transformed with a vector containing At-*OPT3* cDNA or At-*IRT1* cDNA (used here as a positive control). Cell lines were grown on solid medium with or without the Fe chelator bathophenanthroline disulfonate (BPS). All yeast strains grew well on medium without BPS (Figure 3A). In contrast to wild-type cells expressing the empty vector, the *fet3 fet4* mutant expressing the empty vector was not able to grow on medium supplemented with BPS. Consistent with the function of At-IRT1 in high-affinity Fe(II) transport (Eide et al., 1996), its heterologous expression rescued the growth defect of the *fet3 fet4* mutant on Fe-limited medium. Heterologous expression of At-OPT3 partially rescued the growth defect of *fet3 fet4* on Fe-limited medium, suggesting that it might be involved in Fe transport.

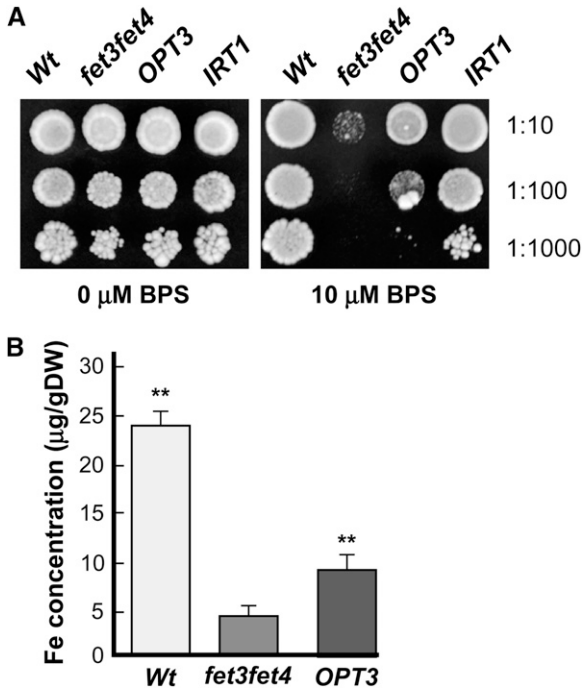

Figure 3. OPT3 Partially Rescues Fe Deficiency of the *fet3 fet4 S. cerevisiae* Mutant.

(A) The wild type and the *fet3 fet4* mutant, transformed with the empty vector (*Wt* and *fet3fet4*, respectively), and the *fet3 fet4* mutant transformed with At-*OPT3* or At-*IRT1* cDNAs (*OPT3* and *IRT1*) were serially 10-fold diluted and spotted onto solid medium supplemented with the indicated concentrations of the Fe chelator BPS. Colonies were visualized after incubating plates for 6 d at 30°C. Dilution series are indicated on the left.

(B) Iron concentration in different *S. cerevisiae* lines, designated as in **(A)**. Shown are mean values ± SE (n = 5 to 8); asterisks indicate statistically significant differences ($P \leq 0.001$) from the empty vector–expressing *opt2* or *fet3 fet4* mutant cells.

We then compared the Fe concentration of the wild-type cells expressing the empty vector with that of the *fet3 fet4* mutant expressing either the empty vector or the vector with At-*OPT3* cDNA. We found that the Fe concentration was 2-fold higher in At-*OPT3*–expressing cells in comparison with *fet3 fet4* cells expressing the empty vector (Figure 3B). We note that in these experiments, cells were grown in medium lacking Fe ligands such as nicotianamine. Therefore, the increased Fe concentration of the At-*OPT3*–expressing cells (Figure 3B) could be due to the ability of At-OPT3 to mediate uptake of Fe ions. This suggestion challenges the prevailing view that At-OPT3 is involved in the transport of peptides, as was shown for other OPT family members (Lubkowitz, 2011).

OPT3 Mediates Transition Ions Transport in *Xenopus laevis* Oocytes

Transport properties of OPT3 were examined in *X. laevis* oocytes. On the onset of uptake studies, we examined the localization of OPT3-GFP in oocytes, characterized electrophysiological properties of *OPT3*-expressing oocytes, and determined suitable uptake conditions. We found that OPT3 resided at the plasma membrane in oocytes, as shown by the localization of the OPT3-GFP–mediated fluorescence at the cell periphery (Supplemental Figure 3). When bathed in ND96 recording solution, oocytes injected with *OPT3* cRNA had significantly less negative resting membrane potentials than control cells in the same ND96 recording solution (Figure 4A), suggesting that the expression of *OPT3* resulted in an OPT3-mediated electrogenic transport. Further investigations were performed by measuring ion transport under voltage clamp conditions, using the conventional two-electrode voltage-clamp method (Figure 4B). In ND96 recording solution, *OPT3*-expressing cells mediated larger inward (i.e., negative) currents relative to those recorded in control cells. Additionally, the *OPT3*-mediated currents reversed at less negative membrane potentials than those recorded in control cells (about −40 mV in contrast to −60 mV observed for control cells; Figure 4C). By convention, the recorded inward (e.g., negative) currents are the product of net positive charge influx (or net negative charge efflux). Although we propose that OPT3 mediates cation influx, the exact nature of the ion(s) carrying the OPT3-mediated current in this ionic environment remains unknown. However, we speculate that under these conditions, the inward currents and decreased resting membrane potential observed in *OPT3*-expressing oocyte cells are the product of a broad substrate specificity of OPT3, which results in OPT3-mediated uptake of the high level of Ca^{2+} present in the ND96-recording solution. Unfortunately, efforts to reduce this large Ca^{2+} background (e.g., 1.8 mM $CaCl_2$) present in the ND96 recording solution below 0.9 mM resulted in an increased activity of endogenous inward currents in control cells (Supplemental Figure 4A). Furthermore, total removal of $CaCl_2$ from the bath solution resulted in the activation of a large endogenous inward conductance (>1 μA at −140 mV) similar to the reported large Ca^{2+}-inactivated

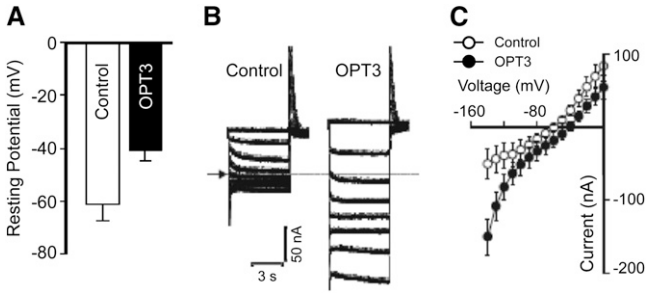

Figure 4. *OPT3* Is Functional in *X. laevis* Oocytes.

(A) Resting membrane potentials of *OPT3*-expressing (*OPT3*) and water-injected (Control) cells measured in standard ND96 recording solution.
(B) Example of OPT3-mediated currents (right panel) elicited in response to holding potentials ranging from 0 to −140 mV (shown only in 20-mV increments for clarity) in standard ND96 recording solution. Endogenous currents recorded in control cells are shown for reference on the left panel. The arrow and dotted line on the left margin indicates the zero current level.
(C) Mean current-voltage (I/V) curves constructed from the steady state currents recordings such as those shown in **(B)** for holding potentials ranging from 0 to −140 mV in 10-mV steps. Error bars represent SE (n = 5).

Cl^- conductance (CaIC) (Amasheh and Weber, 1999). Therefore, based on these preliminary electrophysiological findings, we modified the ionic conditions of the uptake solution to maximize our chances to characterize metal uptake in *OPT3*-expressing oocytes. We maintained 0.9 mM $CaCl_2$ in the medium used for the cation uptake experiments to minimize the activity of endogenous transporters. Likewise, as moderate acidification of the basal uptake media (from 7.5 to 6.0) did not alter the basal transport characteristics of control cells (Supplemental Figure 4B), the pH of the uptake media was adjusted to 6.0. We note that in contrast to control cells, extracellular acidification resulted in a stimulation of the *OPT3*-mediated inward currents, particularly at holding potentials more negative than −100 mV (Supplemental Figure 4C). This is consistent with the proton-coupled nature of OPT-mediated transport (Osawa et al., 2006). Taken together, our data show that OPT3 is functional at the plasma membrane of oocytes, making this heterologous system suitable for cation uptake experiments.

Having established the uptake conditions that would not lead to changes in the endogenous transport in oocytes, we analyzed Fe^{2+} uptake in OPT3-expressing cells. Significant uptake of Fe^{2+} was observed in oocytes expressing *OPT3* cRNA only after 4 h of incubation possibly due to the high endogenous levels of Fe^{2+} found in oocytes (~55 ng/cell) (Figure 5A). Since our electrophysiological studies (Figure 4) suggest that OPT3 might have broad substrate specificity and because Fe transporters such as IRT1 can also transport other divalent metals among which is the toxic metal Cd (Eide et al., 1996), we examined the ability of OPT3 to transport Cd^{2+} ions as well. Differences in Cd^{2+} uptake between control and OPT3-expressing cells were detected after 30 min of incubation of oocytes in the Cd^{2+}-containing uptake solution (Figure 5B), with the magnitude of OPT3-mediated Cd^{2+} uptake increasing in a time-dependent manner. It is worth noting that although these results indicate that OPT3 is capable of mediating the transport of Fe^{2+} and Cd^{2+}, they do not provide an estimate of the relative affinity of the transporter for these ions (e.g., selectivity), which would ultimately determine their role in planta. Nonetheless, these results provide functional proof that OPT3 is a multispecific transporter of transition metal ions unlike other OPT family members that transport peptides.

OPT3 Is Expressed in the Phloem and the Majority of Its Expression Is Associated with the Minor Veins of Leaves and Nodes of Stems

We next examined the cell-type specificity of *OPT3* expression since this knowledge is critical for building the predictive models of the physiological function of OPT3 in planta. Analysis of the expression pattern of *OPT3* in transgenic plants expressing an $OPT3_{pro}$-*GUS* construct revealed β-glucuronidase (GUS) activity predominantly in the vascular tissues of leaves and reproductive organs in *Arabidopsis* (Figures 6A to 6E) and not in roots (Figure 6A), which is consistent with previous findings (Stacey et al., 2006). We noticed, however, that the majority of GUS activity in leaves was localized to minor veins of the vasculature (Figure 6B). We also found the bulk of *OPT3* expression at the nodes of the stem (Figure 6C). Microscopy analysis of the cell-type specificity of *OPT3* expression was conducted in transgenic plants expressing the $OPT3_{pro}$-*GFP* construct. Transverse cross sections through petioles (Figures 6F to 6I) and a nodal section of a stem (Figures 6J to 6M) showed that the majority of $OPT3_{pro}$-*GFP*–mediated fluorescence is associated with the phloem. Consistent with our data, profiling of the translatome of discrete cell populations identified *OPT3* in CCs in leaves (Mustroph et al., 2009). The tissue- and cell-type specificity of *OPT3* expression, along with results from subcellular localization and uptake studies (Figures 1, 3, and 5) suggest that OPT3 may function in

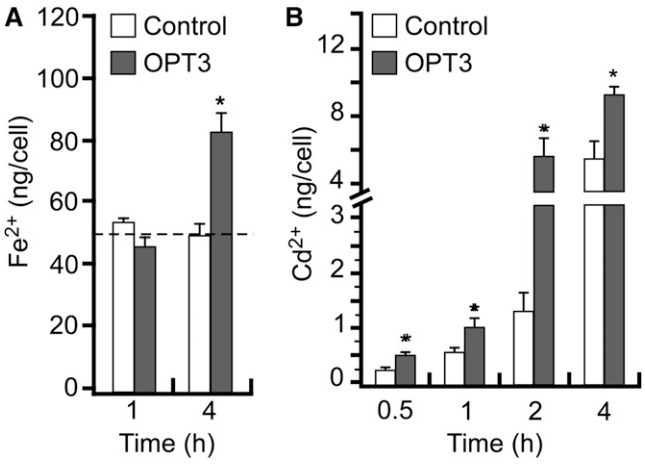

Figure 5. OPT3 Mediates Cation Uptake in *X. laevis* Oocytes.

Uptake of Fe^{2+} **(A)** and Cd^{2+} **(B)** in *OPT3*-expressing oocytes (OPT3) or water-injected cells (Control) at different time points. The basal uptake solution supplemented with 0.4 mM $FeSO_4$ + 1 mM L-ascorbic acid **(A)** or 0.5 mM $CdCl_2$ **(B)**, yielded free extracellular ionic activities of 35 and 150 μM of $\{Cd^{2+}\}_{out}$ and $\{Fe^{2+}\}_{out}$, respectively, as determined by GEOCHEM-EZ (Shaff et al., 2010). The dashed line in **(A)** indicates the basal concentration of endogenous Fe^{2+}. Error bars represent SE (n = 5). Asterisks indicate statistically significant differences ($P \leq 0.05$).

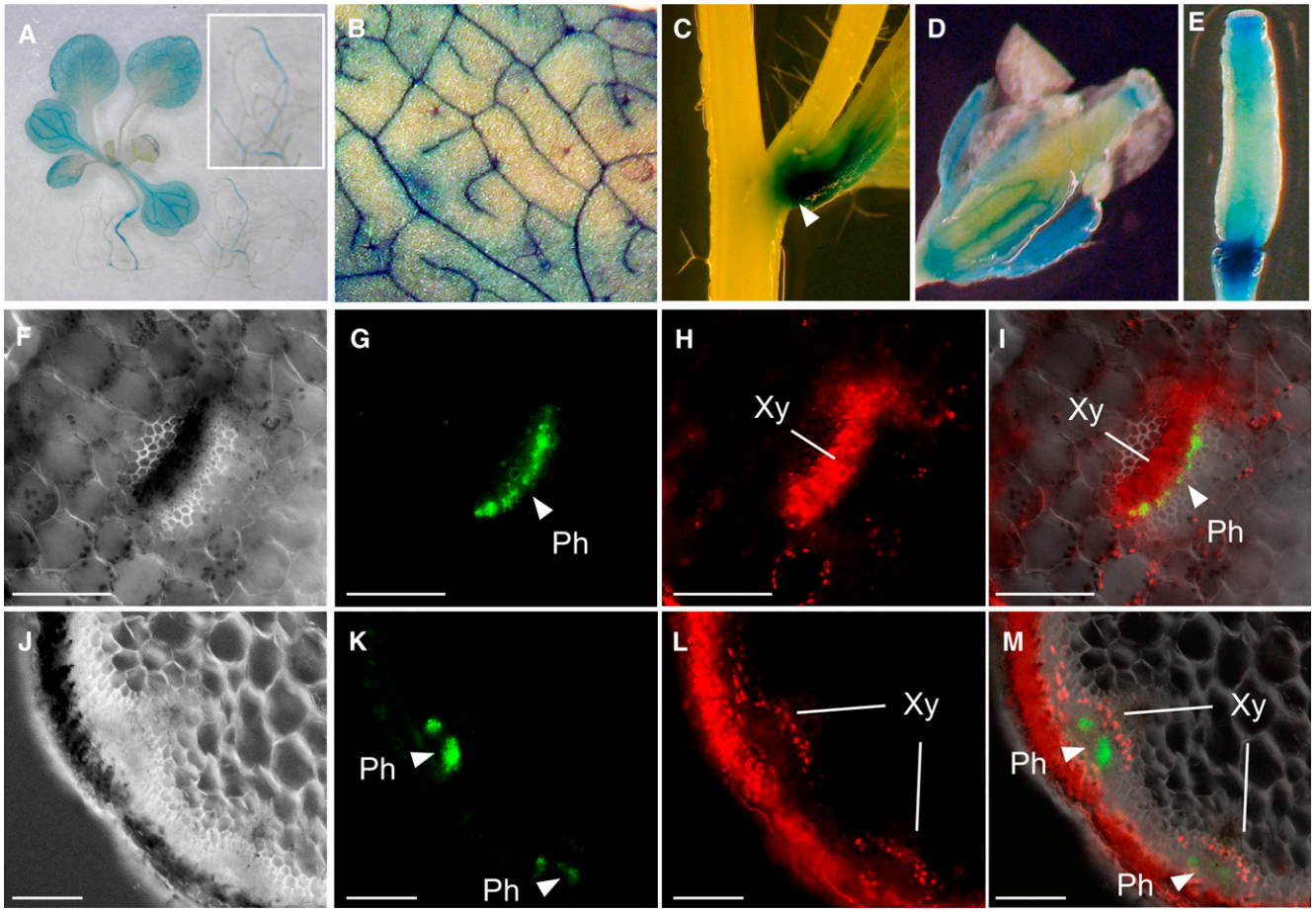

Figure 6. Tissue- and Cell-Type Specificity of *OPT3* Expression in *Arabidopsis*.

(A) to **(E)** Histochemical analysis of the *OPT3* promoter activity in transgenic plants expressing the $OPT3_{pro}$-*GUS* construct.
(A) Representative expression pattern for *OPT3* in a whole seedling. Note the bulk of OPT3 expression in shoots (main figure) but not in roots (inset).
(B) Close-up of the leaf area to demonstrate *OPT3* expression in minor veins.
(C) Expression of *OPT3* at the node (arrow).
(D) and **(E)** Pattern of *OPT3* expression in reproductive organs.
(F) to **(M)** Hand-cut cross sections through the petiole (**[F]** to **[I]**) or inflorescence stem (**[J]** to **[M]**) of 21-d-old transgenic plants expressing the $OPT3_{pro}$-*GFP* construct.
(F) and **(J)** Differential interference contrast images of sections through the petiole and stem at the nodal region, respectively. Overlay images (**[I]** and **[M]**) were created to show that GFP-mediated fluorescence (**[G]** and **[K]**) does not overlap with phenolics-mediated autofluorescence in xylem vessels and chlorophyll-mediated autofluorescence in parenchyma cells (**[H]** and **[L]**). Xy, xylem; Ph, phloem. Bar = 100 μm.

apoplastic loading of transition ions into the phloem companion cells/sieve element complex (CC/SE) for subsequent long-distance transport. In addition, because xylem-to-phloem transfer is suggested to occur at the nodal regions in the stem as well as in minor veins in leaves (Bouche-Pillon et al., 1994; Andriunas et al., 2013), which are the sites of the preferential expression of *OPT3* (Figures 6B and 6C), we hypothesized that OPT3 participates in xylem-to-phloem transfer of transition elements.

Characterization of a Nonlethal Mutant Allele of *OPT3*

To further examine the physiological function of OPT3 in Fe and Cd transport in *Arabidopsis*, we obtained two T-DNA insertion alleles, SALK_021168C (*alias opt3-2*), possessing a T-DNA insertion 36 bp upstream of the *OPT3* start codon (Stacey et al., 2008) and SALK_058794C, designated *opt3-3*, bearing a T-DNA insertion 41 bp upstream of the *OPT3* start codon (Supplemental Figure 5A). Quantitative RT-PCR (qRT-PCR) studies revealed more than 90% reduction of the *OPT3* transcript in plants carrying either allele in comparison with the wild type (Supplemental Figure 5B). We then evaluated the effect of the T-DNA insertion using *opt3-3* mutant plants. Consistent with previous findings with the *opt3-2* allele (Stacey et al., 2008), *opt3-3* mutant plants were smaller than wild-type plants (Supplemental Figure 6A), developed necrotic lesions in cotyledons and older leaves (Supplemental Figures 6B and 6C), had significantly higher concentrations of

Fe compared with the wild type (Supplemental Table 1), and exhibited a constitutive Fe deficiency response that was manifested by increased expression of *IRT1* and *FRO2* (Supplemental Figure 6D). Since *opt3-2* and *opt3-3* mutants exhibited similar phenotypes and fold decreases in *OPT3* transcript abundance, we used the *opt3-3* mutant for subsequent studies.

OPT3 Mediates Partitioning of Fe, but Not Cd, from Source to Sink Tissues

OPT3 is expressed in the phloem, which delivers nutrients, including mineral elements, from source to sink tissues. Therefore, to determine the contribution of OPT3 to Fe, and, possibly, Cd partitioning, we examined concentrations of Fe and Cd in old leaves (sources) and young leaves and seeds (sinks) of the *opt3-3* mutant and wild-type plants. We reasoned that if Fe and Cd are physiological substrates of OPT3, then young leaves and seeds of the *opt3-3* mutant would have a lower concentration of Fe and Cd than young leaves and seeds of wild-type plants.

For analyses of ion concentrations in young and old leaves, we used plants at the late vegetative stage and performed long-term (for Fe; Figure 7A) and short-term (for Fe and Cd; Figures 7B and 7C, respectively) uptake and transport assays. The long-term Fe uptake and accumulation experiment revealed that while there were no significant differences in the concentration of Fe in young and old leaves of wild-type plants, the concentration of Fe was 8-fold higher in old versus young rosette leaves of *opt3-3* mutant plants and 14-fold higher in old leaves when compared with the corresponding leaves in wild-type plants (Figure 7A). Consistent with these data, we were able to detect Fe using the Perls' staining only in old leaves of the *opt3-3* mutant (Supplemental Figure 7). It is noticeable that young leaves of the *opt3-3* mutant accumulated 1.6-fold more Fe than corresponding leaves of the wild type (Figure 7A). This result was not entirely surprising because the Fe concentration in leaves of the *opt3-3* mutant is significantly higher than in the wild type (Supplemental Table 1), which is likely due to increased expression of *IRT1/FRO2* (Supplemental Figure 6D; Stacey et al., 2008). Consistent with the role of OPT3 in

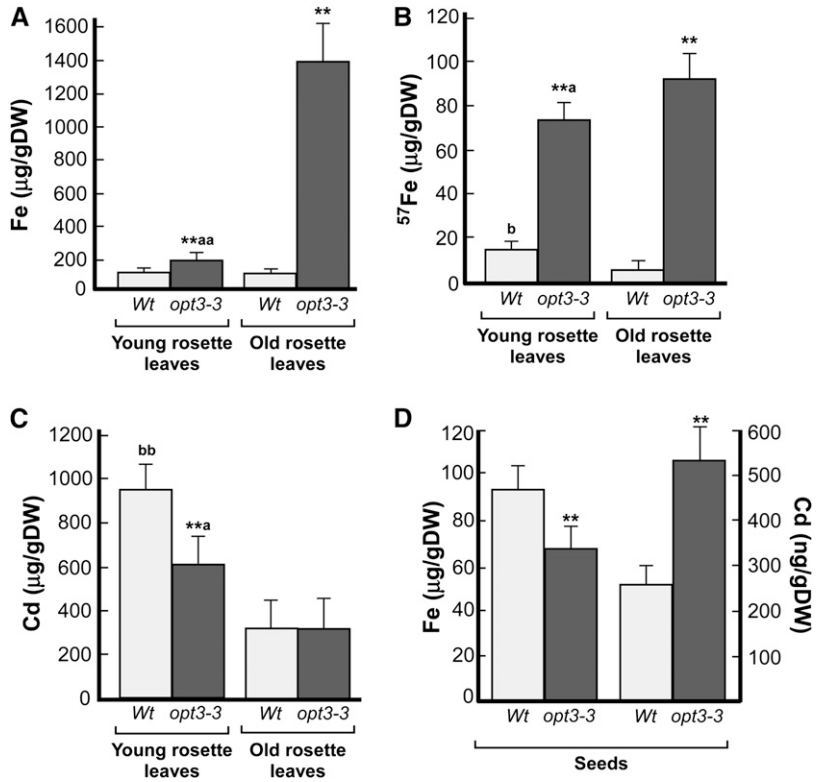

Figure 7. OPT3 Mediates Fe Transport from Source to Sink Tissues.

ICP-MS analysis of Fe and Cd concentrations in old and young leaves (**[A]** to **[C]**) and seeds **(D)** of wild-type and *opt3-3* mutant plants. Asterisks indicate statistically significant differences from the corresponding leaves in the wild type ($P \leq 0.001$). Letters (^{a} and ^{aa}) indicate statistically significant differences between old and young rosette leaves of the *opt3-3* mutant ($^{a}P \leq 0.05$ or $^{aa}P \leq 0.01$). Statistically significant differences between old and young rosette leaves in the wild type are indicated as ($^{bb}P \leq 0.001$). DW, dry weight.

(A) to **(C)** Young and old rosette leaves were harvested at the late vegetative stage from hydroponically grown plants. In **(A)**, plants were grown in 10 μM ^{56}FeHBED (Fe) until tissues were collected for the ICP-MS analysis. In **(B)**, plants were grown in ^{56}Fe until the late vegetative stage and then transferred for 24 h to a fresh hydroponic medium containing 25 μM ^{57}FeHBED (^{57}Fe), while in **(C)**, plants were grown for additional 24 h with 25 μM $CdCl_2$ before sink and source leaves were harvested and subjected to the ICP-MS analysis.

(D) Iron and Cd concentrations in plants grown in soil with 7.5 nM Cd or 10 μM Fe. Error bars represent SE ($n = 3$).

Fe partitioning from source to sink leaves and the fact that young leaves are more susceptible to Fe deficiency (Marschner, 1995), young leaves of the *opt3-2* mutant were more sensitive to Fe deficiency than young leaves of the wild type (Supplemental Figure 8).

In short-term Fe and Cd transport and loading experiments, plants were grown hydroponically until the late vegetative stage and then transferred into a fresh hydroponic medium in which the most common isotope of ^{56}Fe (alias Fe) was replaced with the stable isotope, ^{57}Fe (provided as ^{57}FeHBED [25 μM]), or to hydroponic medium, supplemented with 25 μM $CdCl_2$. After 24 h, roots and shoots were harvested and analyzed for ^{57}Fe and Cd by inductively coupled plasma–mass spectrometry (ICP-MS). In these experiments, young leaves of wild-type accumulated significantly more ^{57}Fe than old leaves (Figure 7B). In contrast, the concentration of ^{57}Fe in young leaves of the *opt3-3* mutant was still significantly lower than in old leaves of the mutant, further supporting the role of OPT3 in Fe partitioning between source and sink tissues. The concentration of ^{57}Fe in young leaves of the *opt3-3* mutant was significantly higher than in young leaves of the wild type as well (Figure 7B). In contrast to ^{57}Fe accumulation pattern, the concentration of Cd was similar in young and old leaves of wild-type and *opt3-3* mutant plants (Figure 7C), suggesting that *opt3-3* might not be involved in the phloem-based remobilization of Cd from source to sink tissues.

We then compared Fe and Cd concentrations in seeds of the wild type and the *opt3-3* mutant, grown in soil with 7.4 nM of Cd or 10 μM Fe. Consistent with previous findings (Stacey et al., 2008), the concentration of Fe in seeds of the *opt3-3* mutant was 1.4-fold lower in comparison with the seeds of wild-type plants (Figure 7D). In contrast, the concentration of Cd in seeds of the *opt3-3* mutant was 2.1-fold higher in comparison with seeds of wild-type plants (Figure 7D). Collectively, these results suggest that OPT3 functions in Fe but not Cd remobilization from source to sink tissues via the phloem in *Arabidopsis*; thus, Fe but not Cd is a physiological substrate of OPT3.

The Phloem Sap of the *opt3* Mutant Contains Less Fe, While the Xylem Sap of the *opt3-3* Mutant Contains More Fe and Less Cd Than the Wild Type

Localization of *OPT3* expression in minor veins of leaves, at the nodal section of stems (Figures 6A and 6B), and in the phloem throughout the plant (Figures 6F to 6M), and the inability of the *opt3-3* mutant to remobilize Fe from the sources to sinks (Figure 7) suggested a function of OPT3 in apoplastic Fe phloem loading and, possibly, xylem-to-phloem Fe transfer along the transport pathway. If this hypothesis is correct, then the concentration of Fe in the phloem would be lower in plants lacking functional OPT3 in comparison with the wild type and, accordingly, the Fe concentration in xylem sap would be higher in *opt3* mutant versus the wild type.

Analysis of phloem sap revealed that the Fe concentration in the phloem was 2.3-fold lower in the mutant than in the wild type (Figure 8A). To ensure that the lower concentration of Fe in the phloem of the *opt3-3* mutant was due to its inability to load Fe into the CC/SE complex rather than lower amounts of phloem exudates, we also compared the concentration of one of the major osmolytes in the phloem, potassium (K), which plays an important role in maintaining hydraulic pressure and pressure flow–based translocation of solutes from source leaves to sink tissues, such as developing leaves, seeds, and roots (Marschner, 1995). Since there was no statistically significant difference between the concentration of K in the phloem of the *opt3-3* mutant and wild-type plants (Figure 8A), we concluded that the decreased Fe concentration in the phloem of the *opt3-3* mutant is due to its inability to load Fe into the CC/SE complex. Due to technical difficulties with phloem sap collection from Cd-treated

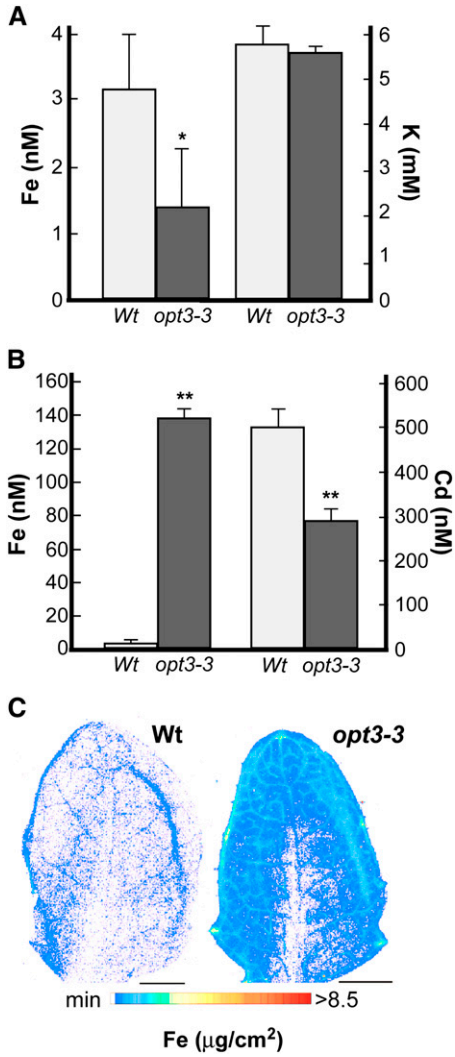

Figure 8. OPT3 Mediates Xylem-to-Phloem Fe Transfer.

(A) and **(B)** The concentration of Fe and K in phloem sap **(A)** or Fe and Cd in xylem sap **(B)**, both collected from wild-type and *opt3-3* mutant plants grown hydroponically under Fe-sufficient conditions. Error bars represent SE (n = 3). Asterisks indicate statistically significant differences (*P ≤ 0.05 and **P ≤ 0.001).

(C) Synchrotron x-ray fluorescence map of Fe distribution in leaves of the wild type and the *opt3-3* mutant in *Arabidopsis*. Note that the line of Fe in the leaf of the wild type is an artifact of the leaf folding. Bar = 1 mm.

plants, we were not able to determine the Cd concentration in the phloem.

Analysis of xylem sap revealed that the concentration of Fe in the sap of the *opt3-3* mutant was 42-fold higher in comparison with the wild type (Figure 8B). This result could be explained using the following not mutually exclusive scenarios: It is possible that lack of an Fe sufficiency signal in the phloem causes upregulation of *FRO2* and *IRT1*, driving enhanced Fe uptake and loading into the xylem. Alternatively, the *opt3-3* mutant may lack the ability to remove Fe from the xylem and load it into the phloem. Consistent with the latter suggestion, analysis of the spatial distribution of Fe using synchrotron x-ray fluorescence microscopy (SXRF) revealed that Fe was associated primarily with the minor veins of the *opt3-3* mutant and was located at the hydathodes and toward the leaf blade periphery, while leaves of the wild type contained significantly less Fe (Figure 8C). Iron was also associated with minor veins of leaves of the *opt3-3* mutant stained with Perls' stain (Supplemental Figure 7). Because minor veins and the leaf periphery are the sites of the preferential expression of *OPT3* (Figure 6B) and are the sites of the intensive xylem-to-phloem transfer (Bouche-Pillon et al., 1994; Turgeon and Webb 1973; Andriunas et al., 2013), we propose that OPT3 loads Fe into the phloem by mediating xylem-to-phloem cycling.

In contrast to Fe, the concentration of Cd was 1.7-fold lower in xylem sap of the mutant in comparison with wild-type plants (Figure 8B). This finding further supports the notion that although OPT3 is capable of transporting Cd ions in vitro, Cd is not the physiological substrate of OPT3 in planta.

Shoots of Cd-Treated the *opt3-3* Mutant Accumulate Less Cd and Are Less Sensitive to Cd Than Shoots of Wild-Type Plants

The decreased concentration of Cd in xylem sap of the *opt3-3* mutant suggests that Cd delivery from roots to shoots might be affected in the mutant, which would result in altered Cd sensitivity. To test this prediction, we grew plants hydroponically to a late vegetative stage and exposed them to Cd for 4 d. We found that roots of the Cd-grown *opt3-3* mutant accumulated significantly more Cd, while leaves accumulated significantly less Cd compared with corresponding organs in wild-type plants (Figure 9A). As a result of the decreased Cd concentration, leaves of the *opt3-3* mutant were less sensitive to Cd than leaves of the wild type, both grown under the same conditions (Supplemental Figure 9).

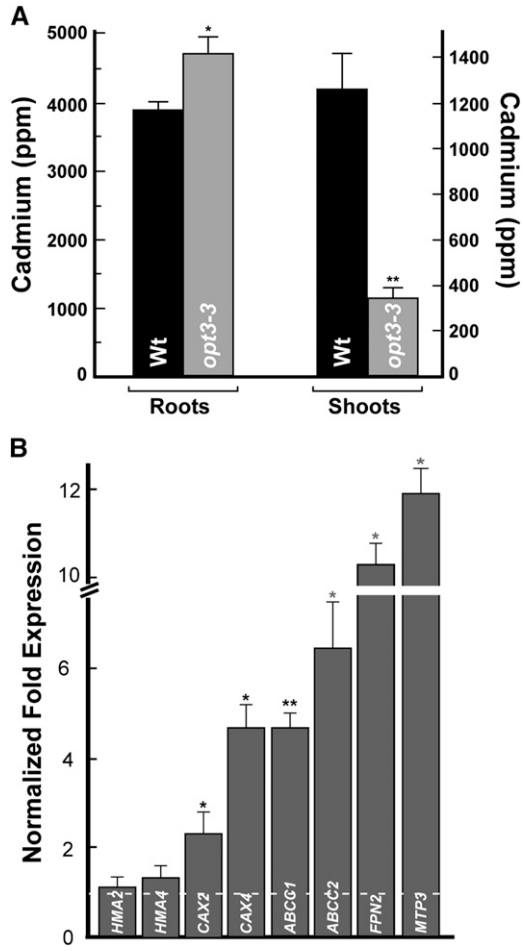

Figure 9. Leaves of *opt3-3* Plants Accumulate Less Cd Than Leaves of Wild-Type Plants.

(A) The concentration of Cd in roots and shoots of wild-type and *opt3-3* mutant plants grown for 4 d with 25 μM $CdCl_2$. Shown are mean values ± SE; $n = 3$. Asterisks indicate statistically significant differences (*P ≤ 0.05 and **P ≤ 0.001).

(B) Transcript abundance of the indicated genes was analyzed in roots of wild-type and *opt3-3* plants, both grown hydroponically to the vegetative stage. Results are presented relative to expression of these genes in roots of wild-type plants designated as 1 (dashed line). Error bars indicate SE ($n = 6$). Asterisks indicate statistically significant differences (*P ≤ 0.05 and **P ≤ 0.001, respectively).

Expression of Vacuolar Heavy Metal Transporters Is Upregulated in Roots of the *opt3-3* Mutant

Given that the *opt3-3* mutant has altered root-to-shoot signaling of Fe deficiency that is manifested by the constitutive upregulation of the expression of *IRT1* and *FRO2* in roots (Supplemental Figure 6D; Stacey et al., 2008), we hypothesized that expression of genes encoding transporters implicated in vacuolar sequestration or xylem loading of Cd might be altered in roots of the *opt3-3* mutant as well. To test this hypothesis, we examined the steady state mRNA level for genes encoding HMA2 and HMA4, which are responsible for Cd loading into the xylem in roots (Wong and Cobbett, 2009), FPN2 (alias IREG2), MTP3, CAX2, and CAX4, which are suggested to play a role in vacuolar heavy metal sequestration (Arrivault et al., 2006; Schaaf et al., 2006; Korenkov et al., 2007), or ABCC1 and ABCC2, which are involved in the vacuolar sequestration of Cd-PC complexes (Park et al., 2012). The qRT-PCR analyses did not reveal statistically significant differences in transcript abundance of *HMA2* and *HMA4* in roots of *opt3-3* versus wild-type plants (Figure 9B). In contrast, transcript abundance of *CAX2*, *CAX4*, *ABCC1*, *ABCC2*, *FPN2*, and *MTP3* were significantly higher in roots of the mutant compared with the wild type. These data suggest that increased abundance of these

and, possibly, other vacuolar heavy metal transporters is among the reasons for Cd retention in roots, decreased Cd loading into the xylem, and accumulation in leaves of the *opt3-3* mutant versus the wild type (Figures 8B and 9A), leading to Cd resistance phenotypes in shoots of the *opt3-3* mutant (Supplemental Figure 9).

DISCUSSION

OPT3 Transports Transition Ions

OPT3 belongs to the oligopeptide transporter family, whose members transport synthetic tetra- and pentapeptides when expressed in heterologous systems; however, the physiological substrates and the physiological role of OPTs, including OPT3, in *Arabidopsis* are unknown (Lubkowitz, 2011). Therefore, after finding that OPT3 localizes to the plasma membrane (Figure 1), we examined if OPT3, similar to is closest homolog from *B. juncea*, Bj-GT1, as well as other OPTs from *Arabidopsis*, would transport GSH. We found that heterologously expressed *OPT3* did not complement the GSH uptake defect of the *Saccharomyces cerevisiae* GSH uptake mutant *opt1* nor did it transport GSH (Figure 2), suggesting that GSH might not be the physiological substrate of OPT3. In contrast, heterologously expressed *OPT3* partially rescued the growth of the *fet3 fet4* mutant in Fe-limited conditions (Figure 3A; Wintz et al., 2003). Importantly, we showed that the ability of OPT3 to rescue Fe deficiency of the *fet3 fet4* mutant is associated with the OPT3-dependent increase in accumulation of Fe in cells of the mutant, even though yeast were grown in medium that lacked the Fe ligand NA (Figure 3B). These data suggested that OPT3 might mediate transport of ions rather than peptides or ion-ligand complexes. Consistent with this suggestion, chelation of Fe^{2+} with the addition of NA to the growth medium abolished the ability of OPT3 to rescue growth of the *fet3 fet4* mutant (Wintz et al., 2003).

The nature of OPT3-mediated transport was examined in *X. laevis* oocytes. After establishing that OPT3 resides at the plasma membrane in oocytes as it does in *Arabidopsis*, we employed uptake conditions that would minimize activation of endogenous oocyte transporters and found that OPT3 likely mediates proton-coupled inward currents as was documented for other OPT family members (Osawa et al., 2006) (Figure 4; Supplemental Figure 4). Subsequently, we showed that OPT3 indeed mediates uptake of Fe^{2+} into *X. laevis* oocytes in a time-dependent manner in medium lacking metal ligands (Figure 5A). Because several characterized Fe transporters have broad substrate specificity, and IRT1 transports Cd in addition to Fe, we also examined whether OPT3 would be able to transport Cd^{2+} ions as well. We found that in addition to Fe, OPT3-mediated Cd^{2+} uptake in *X. laevis* oocytes in medium lacking metal ligands (Figure 5B).

OPT3 Functions in the Translocation of Fe but Not Cd to Sink Organs

To begin the investigation of the role of OPT3 in transition ion transport in planta, we first determined the cell-type specificity of its expression. Using transgenic plants expressing $OPT3_{pro}$-*GUS* or $OPT3_{pro}$-*GFP* fusions, we found that *OPT3* is expressed in minor veins of the vasculature in leaves and nodes of stems and that the bulk of its expression is associated with the phloem (Figures 6B, 6C, and 6F to 6M). Furthermore, *OPT3* was found in CC of the phloem (Mustroph et al., 2009). Because OPT3 mediated Fe and Cd influx in *X. laevis* oocytes as well as Fe accumulation in yeast cells (Figures 3 and 5), we hypothesized that OPT3 is involved in loading of Fe and, possibly, Cd into the CC/SE complex. Because the phloem plays a key role in redistribution of mineral elements from source to sink tissues, we compared Fe and Cd accumulation in older and younger rosette leaves and seeds of the *opt3-3* mutant versus the wild type. We found that the Fe concentration was 8-fold higher in old versus young rosette leaves of *opt3-3* mutant plants, and 14-fold higher in old leaves when compared with the corresponding leaves in wild-type plants (Figure 7A). This result suggested that OPT3 plays a significant role in the delivery of Fe to sink tissues. Because symptoms of Fe deficiency are more prominent in younger tissues (Marschner, 1995), we expected that if OPT3 functions in the phloem-based Fe partitioning then young leaves of the *opt3-3* mutant would be more susceptible to Fe deficiency than young leaves of the wild type. Consistent with this hypothesis, we observed that young leaves of the *opt3-3* mutant were significantly more chlorotic compared with the wild type grown in the same conditions (Supplemental Figure 8). Finally, OPT3 was important for the delivery of Fe to developing seeds (Figure 7D; Stacey et al., 2008). Based on these results, we concluded that OPT3 functions in the phloem-based delivery of Fe to sink tissues and that Fe is a physiological substrate of OPT3.

In contrast to Fe, Cd content was similar in young and old leaves of wild-type and *opt3-3* mutant plants (Figure 7C), suggesting that *opt3-3* might not be involved in the phloem-based remobilization of Cd from source to sink tissues. This suggestion was substantiated by distinctively different kinetics of ^{57}Fe and Cd accumulation in young and old leaves of plants (Figures 7B and 7C) and finding that OPT3 is not involved in Cd loading into seeds (Figure 7D). Together, these results support the notion that although OPT3 can mediate transport of Cd in vitro, it is not involved in Cd partitioning in planta under physiological conditions. It is possible that increased accumulation of Cd in seeds of the mutant versus the wild type is due to the effect of the *OPT3* knockdown on the function/abundance of transporters, such as YSL1 or YSL3, or other transporters that are responsible for metal loading into seeds (Waters et al., 2006; Chu et al., 2010).

The Role of OPT3 in Xylem-to-Phloem Transfer in *Arabidopsis*

It is recognized that young leaves, seeds, and other sink organs receive the majority of their mineral nutrients via the phloem (Marschner, 1995). In addition to symplastic and apoplastic loading of the CC/CE complex, efficient xylem-to-phloem transfer may occur along the long-distance transport pathway with hubs at the nodal regions in the stem and minor veins in the leaf blade (Bouche-Pillon et al., 1994; Andriunas et al., 2013). The companion cells in these places differentiate into transfer cells to enhance membrane transport capacity and phloem loading and redistribution of resources (Andriunas et al., 2013). We found that (1) *OPT3* is expressed in the phloem of minor

veins in leaves and at the nodal sections of the stem (Figure 6), where it is associated with companion cells (Mustroph et al., 2009). (2) The *opt3-3* mutant accumulates Fe in the vicinity of minor veins at the leaf blade periphery (Figure 8C; Supplemental Figure 7), which is suggested to have the strongest source strength (Turgeon and Webb, 1973). (3) OPT3 mediates uptake of Fe ions in yeast and *X. laevis* oocytes (Figures 3 and 5). (4) The xylem sap of the *opt3-3* mutant hyperaccumulates Fe, while phloem sap contains less Fe compared with xylem and phloem saps of the wild type (Figures 8A and 8B). Collectively, these data suggest that OPT3 might contribute to xylem-to-phloem transfer of Fe for subsequent partitioning from source-to-sink tissues.

OPT3 Contributes to Shoot-to-Root Signaling of Fe Status

Revealing the physiological substrate and function of OPT3 has provided fundamental insights that have implications for the nature and mechanism of systemic Fe signaling in plants (summarized in Figure 10). First, our finding that the concentration of Fe is significantly lower in the phloem sap of the *opt3-3* mutant (Figure 8A), which overexpresses *IRT1* and *FRO2* in the root even under Fe-sufficient conditions, provides experimental evidence that is consistent with the hypothesis that Fe availability in the phloem is essential for the regulation of Fe deficiency responses in the root. Second, it has been suggested that OPT3 plays a role in communicating Fe status from shoots to roots (Stacey et al., 2008), and we provide a mechanistic basis for this phenomenon where OPT3 mediates Fe recirculation from the xylem to the phloem (Figure 8). Loss of this ability results in Fe hyperaccumulation in leaves of *opt3* knockdown mutants (Supplemental Table 1; Stacey et al., 2008). The mechanistic explanation of foliar Fe hyperaccumulation phenotypes of the *opt3* knockdown mutant provided by our data also rationalize findings by García et al. (2013) that foliar application of Fe rescues constitutive Fe acquisition responses manifested in roots of the *Arabidopsis frd3*, pea *brz*, and tomato *chln* mutants, but not in the root of the *opt3-2* mutant. We reason that knockdown of *OPT3* results in plants incapable of loading Fe into the phloem for the long-distance transport into the root; thus, foliar application of Fe does not rescue its Fe deficiency responses. In contrast, we found that grafting wild-type shoots onto *opt3-3* mutant roots downregulated *FRO2* and *IRT1* expression relative to their expression in control grafts (wild-type shoots onto wild-type roots) (Supplemental Figure 10A). This finding emphasizes that OPT3-mediated Fe transport function in the shoot is sufficient to regulate the transcriptional Fe deficiency responses in the root. Consistent with the suggestion that OPT3 function is required in shoots, its transcript abundance in shoots was 10-fold higher than in roots of wild-type plants (Supplemental Figure 10B). Collectively, these data provide molecular evidence that Fe availability in the phloem regulates expression of Fe acquisition genes in the root and identify OPT3 as an important contributor to the systemic signaling of Fe status.

Our data also suggest that the decreased Cd concentration in xylem sap and shoots of the *opt3-3* mutant and increased Cd tolerance of leaves of the mutants versus the wild type (Figures 8B and 9A; Supplemental Figure 9) is a consequence of OPT3 contribution to phloem-based systemic Fe signaling (Figure 10). Indeed, we found that expression of genes encoding transporters that are implicated in vacuolar sequestration of Cd ions (FPN2, CAX2, CAX4, and MTP3) and vacuolar sequestration of Cd-PC complexes (ABCC1 and ABCC2) is significantly upregulated in roots of the *opt3-3* mutant versus the wild type (Figure 9B). We hypothesize that these and possibly other transporters contribute to the retention of Cd in roots of the *opt3-3* mutant, subsequently affecting Cd loading into the xylem, root-to-shoot Cd partitioning, and increasing Cd tolerance of the shoot.

In conclusion, data presented in this article uncovered a central role of OPT3 in Fe loading into the phloem, provided mechanistic explanation of OPT3-mediated shoot-to-root communication of Fe status in *Arabidopsis*, and highlighted the role of Fe in the phloem-based systemic signaling, a long-debated area in plant

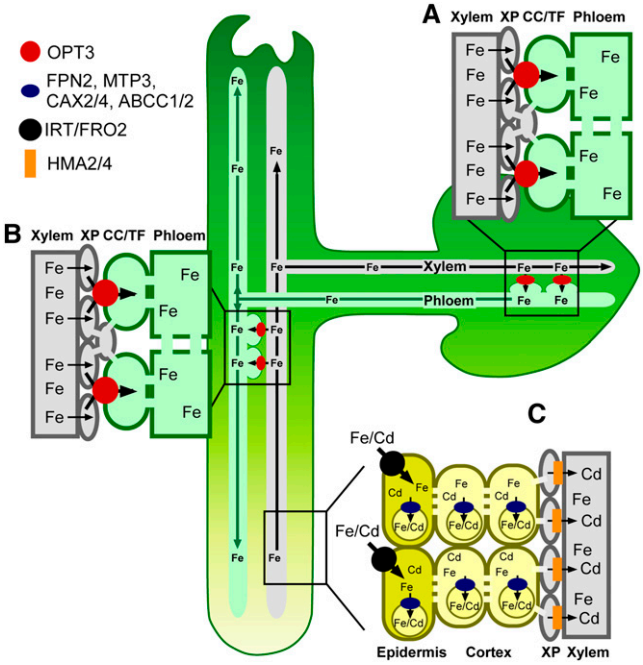

Figure 10. Model of OPT3 Function in *Arabidopsis*.

This figure summarizes the proposed dual roles of OPT3 in the redistribution of Fe from source to sink tissues, in shoot-to-root signaling of shoot Fe status and its contribution to Cd partitioning in *Arabidopsis*.
(A) *OPT3* is expressed in CCs of the phloem that might differentiate into the transfer cells (TF) in minor veins of leaves and in nodes of stems. In these sites, OPT3 facilitates Fe loading into the phloem, possibly by direct xylem-to-phloem Fe transport.
(B) At the whole-plant level, OPT3 is involved in redistribution of Fe from sources to sinks and Fe recirculation into roots. Iron recirculation into roots via OPT3 plays a signaling role by conveying Fe status of the shoot.
(C) Although OPT3 transports Cd in vitro, it is likely that it mediates root-to-shoot partitioning of Cd indirectly by orchestrating shoot-to-root Fe signaling that, in turn, alters expression of genes encoding multispecific transition ion transporters (e.g., FPN2, MTP3, CAX2/4, ABCC1/2, and possibly others). These transporters facilitate vacuolar sequestration of Cd and its retention in the root, which in turn, affects root-to-shoot Cd partitioning and Cd resistance. XP, xylem parenchyma cells.

Fe homeostasis research. Our results also indicate that OPT3 contributes to Fe recycling from the xylem and acts as a functional link between the xylem and the phloem. We show that OPT3 is a multispecific transition element transporter. This functional activity distinguishes OPT3 from other peptide-transporting OPT family members. Given the acute Fe deficiency responses of *OPT3* knockdown and knockout mutants, and the indirect effect of OPT3 on Cd partitioning in *Arabidopsis*, we propose that Fe, but not Cd, is a physiological substrate of OPT3, although it is capable of transporting both Cd^2 and Fe^{2+} ions when expressed in *X. laevis* oocytes. Another important implication from this work is finding that loss of *OPT3* function significantly decreases Fe while increasing Cd concentration in seeds, suggesting that manipulation of the expression of this transporter can provide promising avenues for targeted biofortification strategies directed at increasing Fe density, while omitting Cd, in the edible portions of crops.

METHODS

Plant Material and Growth Conditions

All plant lines used in the study were in the *Arabidopsis thaliana* Columbia background. Seeds of *opt3-2* (SALK_021168C) and *opt3-3* (SALK_058794C) T-DNA insertion alleles were obtained from the ABRC (Alonso et al., 2003). The *opt3-2* allele is also described (Stacey et al., 2002, 2008). *opt3-2* and *opt3-3* homozygous lines were identified by PCR using the left border T-DNA–specific and the gene-specific primers (Supplemental Table 2).

For growing plants in hydroponics, 8-d-old seedlings were transferred from half-strength Murashige and Skoog (MS) agar plates to *Arabidopsis* hydroponic solution described by Arteca and Arteca (2000). The hydroponic solution was changed every 5 d. For Fe deficiency assays, plants were grown hydroponically for 3 weeks and transferred to medium without FeHBED for the indicated time. In all experiments, the growth conditions were as follows: 12-h-light/12-h-dark photoperiod (at a photosynthetic photon flux density of 120 μmol photons m^{-2} s^{-1}) at 23°/19°C light/dark temperature regime and 75% relative humidity.

Subcellular Localization and Fluorescent Microscopy

The full-length *OPT3* cDNA was isolated by RT-PCR using total RNA from wild-type *Arabidopsis* leaves and primers sets that would introduce *attB* sites on the resulting PCR product (Supplemental Table 2). The PCR product was introduced into the DONR222 entry vector (Invitrogen) before recombination cloning into the GWB406 destination vector (Nakagawa et al., 2007) to fuse GFP in frame with the N termini of OPT3 under the control of the cauliflower mosaic virus 35S promoter. The resulting *$35S_{pro}$-OPT3-GFP* construct or GWB406, lacking the cDNA insert, was transfected into *Arabidopsis* protoplasts (Zhai et al., 2009). GFP-mediated fluorescence and chlorophyll autofluorescence were visualized using fluorescein isothiocyanate (FITC) or rhodamine filter sets, respectively, of an Axio Imager M2 microscope equipped with the motorized Z-drive (Zeiss). Z-stack (1.3 μm thick) images were collected with the high-resolution AxioCam MR camera and then 3D deconvoluted using an inverse filter algorithm of the Zeiss AxioVision 4.8 software.

Expression of *OPT3-GFP* in Onion Epidermal Cells

For visualizing OPT3 localization in onion (*Allium cepa*) cells, the *$35S_{pro}$-OPT3-GFP* construct in the GWB406 vector and the plasma membrane marker PIP2A fused to mCherry in the BIN vector (Nelson et al., 2007) were introduced into onion epidermal cells by biolistic transformation as described (Jung et al., 2012). Briefly, 2 μg of each construct in 10 μL of distilled water was mixed with 10 μL of solution containing 50 mg/mL of 1.0-μm gold particles, 10 μL of 2.5 mM $CaCl_2$, and 4 μL of 0.1 M spermidine. The mixture was incubated for 30 min at room temperature. Gold particles coated with plasmid DNAs were rinsed with cold ethanol and then gently suspended in 20 μL of ethanol. Onion pieces were placed onto agar plates containing 1× MS medium and bombarded using a double-barreled extension of the Bio-Rad He/1000 particle delivery system (PDS-1000/He) with 1100 p.s.i. rupture discs under a vacuum of 0.04 bar. Onion pieces were left to recover after bombardment in the dark at 25°C for 16 h. Onion skin epidermal layers were peeled from the onion pieces and placed on glass slides for analyses. When indicated, onion epidermal cells were plasmolyzed by incubating in 20% (w/v) sucrose solution for 10 min.

Tissue- and Cell-Type Specificity of *OPT3* Expression in *Arabidopsis*

A 3.5-kb genomic fragment including sequence upstream of *OPT3* start codon was amplified by PCR using indicated primer pairs (Supplemental Table 2). The resulting amplicon was fused to the bacterial *uidA* gene encoding GUS of the GUS1-Gate vector (Jung et al., 2012) or to GFP of the YXT2 destination vector (Xiao et al., 2010). The resulting *$OPT3_{pro}$-uidA* (*$OPT3_{pro}$-GUS*) or *$OPT3_{pro}$-GFP* constructs were transformed into wild-type *Arabidopsis* (Clough and Bent, 1998). GUS staining was performed for 16 h with 2 mM X-Gluc (5-bromo-4-chloro-3-indolyl-β-D-glucuronide) as described (Jefferson et al., 1987). Staining patterns were analyzed using Leica S6E stereomicroscope. Hand-cut sections were prepared from stems and petioles of transgenic *Arabidopsis* plants expressing *$OPT3_{pro}$-GFP* using a feather double-edge razor blade. GFP and autofluorescence were visualized using FITC (for GFP) or rhodamine (for autofluorescence) filter sets of the Axio Imager M2 microscope equipped with the motorized Z-drive (Zeiss). Images were processed using the Adobe Photoshop software package, version 12.0.

Functional Complementation Assays in *Saccharomyces cerevisiae*

S. cerevisiae strains used in this study were BY4741 (MATa; his3Δ1; leu2Δ0; met15Δ0; ura3Δ0); opt1(alias ABC822) (*MATa; ura3-52; leu2Δ1; lys2-801; his3Δ200; trp1Δ63; ade2-101; hgt1Δ::LEU2*); DY1457 (*MATa ade6 can1 his3 leu2 trp1 ura3*); and DEY1453 (*MATa/MATα ade2/+ canI/canI his3/his3 leu2/leu2 trpI/trpI ura3/ura3 fet3-2::HIS3/fet3-2::HIS3fet4-1::LEU2/fet4-1::LEU2*). For details of functional complementation assays, see the Supplemental Methods. Briefly, the full-length *OPT3* or *IRT1* cDNAs were cloned by recombination into YES3-Gate vector, and resulting vectors, YES3-Gate-OPT3, YES3-Gate-IRT1, and YES3-Gate, lacking the cDNA insert, were transformed into different yeast strains using the Frozen-EZ yeast Transformation II Kit (Zymo Research).

To test if OPT3 would rescue GSH uptake deficiency of the *opt1* mutant in medium with GSH as the only sulfur (S) source, the *opt1* mutant expressing either *OPT3* or the empty vector were grown in YNB medium with supplements to an OD_{600} = 1.2. Cells were then washed in ice-cold water three times and inoculated (1:200) into SC-S media supplemented with 200 μM of GSH. SC-S was prepared according to the YNB recipe (Bacto Yeast Nitrogen Base without amino acids and ammonium sulfate; DIFCO Laboratories), with the modification that all sulfur containing reagents in macroelements and microelements were substituted with equal amounts of the corresponding chloride salts (Zhang et al., 2004). The medium was supplemented with His, Trp, Ade, and Lys.

For functional complementation assays in the *fet3 fet4* Fe uptake-deficient mutant, YES3-Gate-OPT3, YES3-Gate-IRT1, and YES3-Gate lacking cDNA inserts were transformed into the *fet3 fet4* mutant or the empty vector was transformed into the wild-type strain DY1457. The transformants were selected on YNB medium (pH 4.0) lacking uracil but

supplemented with adenine sulfate (20 mg/L), tryptophan (20 mg/L), and ferric chloride (10 μM). Yeast colonies were inoculated into the same liquid medium and grown overnight to an OD_{600} of 1.0. Yeast cells were washed in sterile water to desorb excess $FeCl_3$ from cell walls and aliquots of cell suspension were serially diluted and spotted onto solid YNB medium (pH 4.0) lacking uracil but supplemented with adenine sulfate (20 mg/L), tryptophan (20 mg/L), and 10 μM BPS. Colonies were visualized after incubating plates for 6 d at 30°C.

Elemental Analysis

Elemental composition was analyzed in *Arabidopsis* and *S. cerevisiae*. For studies in *Arabidopsis*, plants were grown hydroponically as described above. In long-term experiments of Fe accumulation in old and young leaves, plants were grown until the late vegetative stage. For short-term Fe and Cd uptake and transport studies, plants were grown in 10 μM of Fe-HBED (in ^{56}Fe as common isotope of Fe, natural abundance 91.7%) until the late vegetative stage and then transferred for an additional 24 h to a fresh hydroponic medium in which ^{56}Fe was replaced with 25 μM ^{57}Fe (Isoflex USA; 95% enrichment) or to a fresh hydroponic medium supplemented with 25 μM $CdCl_2$ for 24 h before sink and source leaves were harvested and subjected to the ICP-MS analysis. Roots and leaves were harvested and roots were desorbed of Cd and Fe as well as other elements by washing with 10 mM EDTA followed by washing in a solution with 0.3 mM bathophenanthroline disulphonate and 5.7 mM sodium dithionite and then rinsed with deionized water. Shoots were rinsed with deionized water. In analyses of Fe and Cd accumulation in young and old leaves, the two bottommost rosette leaves (old) and uppermost rosette leaves >3 mm (young) were collected from three to five plants. For analyses of Fe and Cd concentration in seeds, plants were grown in soil with 7.4 nM Cd or 10 μM Fe. Elemental analysis was performed using ICP-MS as described (Lahner et al., 2003). The ICP-MS–based analysis of the Fe concentration in yeast cells was performed as described (Jung et al., 2012; Gayomba et al., 2013) except that liquid YNB media used for growing yeast cells was at pH 4.0, was lacking uracil, and was supplemented with adenine sulfate (20 mg/L), tryptophan (20 mg/L), and 10 μM $FeCl_3$.

Expression of *OPT3* in *Xenopus laevis* Oocytes and Electrophysiological Recordings

The coding region of *OPT3* was cloned into the T7TS plasmid (Cleaver et al., 1996), at the *Eco*RV unique site flanked by the 3′ and 5′ untranslated regions of a *X. laevis β-globin* gene. The construct was fully sequenced and checked for sequence accuracy. cRNA was synthesized from 1 μg *Sma*I-linearized plasmid DNA template using a mMessage in vitro transcription kit (Ambion) according to the manufacturer's recommendations and stored at −80°C. Stage V to VI *X. laevis* oocytes were harvested, defolliculated, and cultured in ND96 solution containing 96 mM NaCl, 2 mM KCl, 1.8 mM $CaCl_2$, 1 mM $MgCl_2$, 2.5 mM Na-pyruvate, 50 μg/mL gentamycin, 0.4 mg/mL BSA, and 5 mM HEPES/NaOH to adjust pH to 7.5, as described previously (Piñeros et al., 2008). *X. laevis* oocytes were injected with 50 nL of water (control) or 50 nL of water containing 50 ng of *OPT3* cRNA and incubated in ND96 solution at 18°C for 2 to 4 d prior to the uptake and electrophysiological measurements.

Electrophysiological recordings were done under constant bath perfusion with both GeneClamp 500 and Axoclamp 900A amplifiers (Axon Instruments) using the two-electrode voltage-clamp technique. Recording electrodes were filled with 0.5 M K_2SO_4 and 30 mM KCl and had resistances between 0.5 and 1.5 MΩ. Cells were bathed under constant perfusion in a ND96-recording solution consisting of (in mM) 96 NaCl, 1 KCl, and 1.8 $CaCl_2$ with the pH adjusted to 7.5 with 5 mM HEPES/NaOH. Given the presence of variable endogenous inward current at hyperpolarizing holding potentials (Amasheh and Weber, 1999; Kuruma et al., 2000) currents under voltage clamp conditions were elicited by a 6-s voltage pulses (in 10-mV step increments) restricted between 0 and −140 mV, with a 2-s rest at 0 mV between each voltage pulses. The output signal was digitized and analyzed using Digidatas 1320A and 1440A PClamp 10 data acquisition systems (Axon Instruments). The steady state current-voltage (I/V) relationships were constructed by measuring the current amplitude at the end of the test pulse. All data points represent the mean of at least eight different cells from three to four donor frogs. Error bars denote SE and are not shown when they are smaller than the symbol.

Metal Uptake in Oocytes

The basal uptake solution consisted of a modified ND96 solution containing 96 mM NaCl, 1 mM KCl, and 0.9 mM $CaCl_2$, buffered with 5 mM MES/NaOH to pH 6.0. The uptake solutions was supplemented with 0.5 mM $CdCl_2$ or 0.4 mM $FeSO_4$ + 1 mM L-ascorbic acid (freshly prepared) to prevent Fe oxidation. Given the strong interaction of Cd with Cl (e.g., 80% of the Cd present in the uptake solution is complexed with Cl), the free Cd^{2+} activity in the uptake solution was estimated to be 35 μM Cd^{2+}, while Fe^{2+} free activity was 150 μM as determined by GEOCHEM-EZ (Shaff et al., 2010). Each sample contained six oocytes, with five replicates per time point. At a given time point, the uptake was terminated by washing oocytes through six consecutive ice-cold basal uptake solution. Samples were digested in 100 μL of 70% $HClO_4$, resuspended in 10 mL of 0.1 M nitric acid, and analyzed using ICP-MS (Perkin-Elmer Sciex). Uptake data are expressed "per oocyte" and are representative of at least five independent experiments.

Collection and Analysis of Xylem Sap

Xylem sap was collected as previously described (Sunarpi et al., 2005). Briefly, wild-type and *opt3-3* mutant plants were cultured on hydroponic media until the late vegetative stage. For analyses of Cd concentration, plants were subjected to 25 μM $CdCl_2$ for 48 h. After removal of rosette leaves, the inflorescence stem was cut with a fresh razor blade. Xylem sap exudation was facilitated through a high humidity environment by covering the plants with a plastic dome. The first droplets were excluded to avoid contamination and then xylem sap was collected quantitatively with a micropipette. Cadmium and Fe concentrations in the sap were analyzed by ICP-MS and normalized per volume of the collected sample.

Collection and Analysis of Phloem Sap

Phloem sap was collected from hydroponically grown wild-type and *opt3-3* mutant plants at the late vegetative stage. To prevent entrance of air bubbles into the vasculature, whole rosettes were removed from the root using a razor blade and immersed in deionized water before individual leaves were detached at the petiole. Three leaves (leaf numbers 9 and 10) collected from one plant were pooled together and flushed of xylem sap by placing the petioles in a tube filled with 300 μL of deionized water and incubated in an illuminated growth chamber for 15 min before further incubation in darkness for 1 h. The petioles were then recut under 5 mM Na_2-EDTA (pH 7.5) under low light before placing the petioles in 250 μL of 5 mM Na_2-EDTA (pH 7.5). The leaves where then incubated in darkness for 1 h in a high-humidity chamber lined with wet paper towels and sealed with Vaseline. Samples were diluted with 5 mL of 5% HNO_3 for subsequent detection of K or Fe by ICP-MS.

SXRF

Wild-type and *opt3-3* mutant plants were grown on solid half-strength MS medium for 23 d. Fully developed leaves (second from the bottom) were detached immediately prior to analysis using Teflon-coated forceps and placed adaxial side uppermost, on 35-mm slide mounts across which Kapton metal-free tape was stretched. The distribution of Fe in hydrated

leaf tissue was imaged via SXRF with hard x-ray microprobe X26A of the National Synchrotron Light Source as detailed in the Supplemental Methods.

Perls' Staining

Ferric iron was visualized in leaves of *Arabidopsis* using Perls' staining as described (Green and Rogers, 2004). Briefly, wild-type and *opt3-3* mutant plants were grown hydroponically in Fe-replete conditions until the late vegetative stage. Shoots from 5-week-old hydroponically grown wild-type and *opt3-3* plants were vacuum infiltrated with Perls' stain solution (4% HCl [v/v] and 4% [w/v] potassium ferrocyanide) and allowed to incubate under vacuum for 1 h. Samples were then removed from the vacuum chamber and incubated for 1.5 h. The reaction was stopped by rinsing samples three times with distilled water.

Reciprocal Grafting

Five- or seven-day-old seedlings were used for grafting experiments, performed as described (Rus et al., 2006). After recovery for 5 d, robust grafts lacking adventitious roots on the scion were transferred to hydroponics and cultured for 2.5 weeks before $CdCl_2$ (25 μM) was added to the hydroponic medium. Grafts were photographed and tissues were collected at the indicated time points. RNA for qRT-PCR analysis was isolated from roots of grafted plants grown to the late vegetative stage.

RNA Isolation and qRT-PCR

Arabidopsis wild-type and *opt3-3* mutant plants were grown hydroponically until late vegetative stage. Total RNA was isolated from roots and shoots of hydroponically grown plants using the Trizol reagent (Invitrogen) according to the manufacturer's recommendations. DNase I (Roche) digestion of genomic DNA prior to first-strand cDNA synthesis and qRT-PCR thermocycling procedures were as described (Jung et al., 2012; Gayomba et al., 2013). Data were normalized to the expression of *F14F8.90* (*AT5G15710*) and *ACTIN2* (*AT3G18780*). The fold difference ($2^{-\Delta\Delta Ct}$) or relative quantities were calculated using the CFX Manager Software, version 1.5 (Bio-Rad).

Statistical Analysis

Statistical analyses of the majority of experimental data were performed using the ANOVA single-factor analysis. Statistical analysis of qRT-PCR data was performed using the Relative Expression Software Tool (Qiagen; Pfaffl et al., 2002).

Accession Numbers

Sequence data from this article can be found in the GenBank/EMBL libraries under the following accession numbers (accession numbers in parenthesis): At-*OPT3* (AT4G16370), At-*FIT1* (AT2G28160), At-*IRT1* (AT4G19690), At-*FRO2* (AT1G01580), At-*HMA2* (AT4G30110), At-*HMA4* (AT2G19110), At-*FPN2* (AT5G03570), At-*ACT2* (AT3G18780), At-*F14F8.90* (AT5G15710), At-*CAX2* (AT3G13320), At-*CAX4* (AT5G01490), At-*ABCC1* (AT1G30400), At-*ABCC2* (AT2G34660), At-*MTP3* (AT3G58810), and Sc-*OPT1* (NM_001181645)

Supplemental Data

The following materials are available in the online version of this article.

Supplemental Figure 1. OPT3-GFP Localizes to the Plasma Membrane in Epidermal Onion Cells.

Supplemental Figure 2. *OPT3* Does Not Alter Growth of the *opt1* Mutant of *S. cerevisiae* under Control Conditions.

Supplemental Figure 3. OPT3 Localizes to the Plasma Membrane in *X. laevis* Oocytes.

Supplemental Figure 4. Electrophysiological Properties of *X. laevis* Oocytes Expressing *OPT3*.

Supplemental Figure 5. T-DNA Insertions Upstream of the OPT3 Start Codon Reduce the *OPT3* Transcript.

Supplemental Figure 6. The *opt3-3* Knockdown Allele (*opt3-3*) Exhibits Constitutive Fe Deficiency Symptoms.

Supplemental Figure 7. Iron Localizes at Minor Veins of Old Rosette Leaves in the *opt3-3* Mutant (*opt3-3*).

Supplemental Figure 8. Young Leaves of the *opt3-3* Mutant Are More Sensitive to Fe Deficiency Than Corresponding Leaves of Wild-Type Plants.

Supplemental Figure 9. Leaves of *opt3-3* Plants Accumulate Less Cd and Are Less Sensitive to Cd Than Leaves of the Wild-Type.

Supplemental Figure 10. OPT3 Functions Primarily in Shoots in *Arabidopsis*.

Supplemental Table 1. Leaf Element Profile of the Wild-Type and the *opt3-3* (*opt3-3*) Allele.

Supplemental Table 2. List of Oligos.

Supplemental Methods.

Supplemental References.

ACKNOWLEDGMENTS

We thank Walter Gassmann (University of Missouri) and Serge Delrot (University of Bordeaux, France) for *S. cerevisiae* mutant strains; Christopher D. Town (J. Craig Venter Institute) for the *YXT2* vector; Julian Schroeder (University of California, San Diego) and David Mendoza-Cozatl (University of Missouri) for discussing the cell-type specificity of *OPT3* expression; the Scanlon Lab (Cornell University) for help with *Arabidopsis* tissue sectioning; and the Turgeon Lab (Cornell University) for discussing phloem exudate collection. SXRF studies were performed at Beamline X26A, National Synchrotron Light Source (NSLS), Brookhaven National Laboratory. X26A is supported by the Department of Energy-Geosciences (DE-FG02-92ER14244 to the University of Chicago-CARS). Use of the NSLS was supported by the Department of Energy under Contract DE-AC02-98CH10886. Work in the Vatamaniuk lab was supported by the National Science Foundation (MCB-0923731) and Cornell University Agricultural Experiment Station CUAES Hatch (NYC-125433). Work in the Guerinot lab was funded by the Division of Chemical Sciences, Geosciences, and Biosciences, Office of Basic Energy Sciences of the U.S. Department of Energy through Grant DE- FG02-06ER15809, and work in the Salt lab was funded by the U.S. National Science Foundation through Grant IOS 0701119.

AUTHOR CONTRIBUTIONS

Z.Z., H.J., S.R.G., N.K.V., M.P., and O.K.V. designed experiments. D.E.S., M.L.G., and L.V.K. contributed to discussion on the article and provided analytical tools for the article. Z.Z., H.J., S.R.G., M.P., N.K.V., M.R., T.P., E.C., B.L., and J.D. performed experiments. The article was written by O.K.V., S.R.G., and M.P. All authors analyzed data and contributed constructive comments on the article.

Received January 29, 2014; revised March 31, 2014; accepted April 22, 2014; published May 27, 2014.

REFERENCES

Alonso, J.M., et al. (2003). Genome-wide insertional mutagenesis of *Arabidopsis thaliana.* Science **301:** 653–657.

Amasheh, S., and Weber, W. (1999). Further characteristics of the $Ca(^{2+})$-inactivated $Cl(^{-})$ channel in *Xenopus laevis* oocytes. J. Membr. Biol. **172:** 169–179.

Andriunas, F.A., Zhang, H.-M., Xia, X., Patrick, J.W., and Offler, C.E. (2013). Intersection of transfer cells with phloem biology-broad evolutionary trends, function, and induction. Front Plant Sci **4:** 221.

Arrivault, S., Senger, T., and Krämer, U. (2006). The *Arabidopsis* metal tolerance protein AtMTP3 maintains metal homeostasis by mediating Zn exclusion from the shoot under Fe deficiency and Zn oversupply. Plant J. **46:** 861–879.

Arteca, R.N., and Arteca, J.M. (2000). A novel method for growing *Arabidopsis thaliana* plants hydroponically. Physiol. Plant. **108:** 188–193.

Baxter, I.R., Vitek, O., Lahner, B., Muthukumar, B., Borghi, M., Morrissey, J., Guerinot, M.L., and Salt, D.E. (2008). The leaf ionome as a multivariable system to detect a plant's physiological status. Proc. Natl. Acad. Sci. USA **105:** 12081–12086.

Bogs, J., Bourbouloux, A., Cagnac, O., Wachter, A., Rausch, T., and Delrot, S. (2003). Functional characterization and expression analysis of a glutathione transporter, BjGT1, from *Brassica juncea*: evidence for regulation by heavy metal exposure. Plant Cell Environ. **26:** 1703–1711.

Bouche-Pillon, S., Fleurat-Lessard, P., Fromont, J.C., Serrano, R., and Bonnemain, J.L. (1994). Immunolocalization of the plasma Mmembrane H^{+}-ATPase in minor veins of *Vicia faba* in relation to phloem loading. Plant Physiol. **105:** 691–697.

Bourbouloux, A., Shahi, P., Chakladar, A., Delrot, S., and Bachhawat, A.K. (2000). Hgt1p, a high affinity glutathione transporter from the yeast *Saccharomyces cerevisiae.* J. Biol. Chem. **275:** 13259–13265.

Cagnac, O., Bourbouloux, A., Chakrabarty, D., Zhang, M.-Y., and Delrot, S. (2004). AtOPT6 transports glutathione derivatives and is induced by primisulfuron. Plant Physiol. **135:** 1378–1387.

Chu, H.H., Chiecko, J., Punshon, T., Lanzirotti, A., Lahner, B., Salt, D.E., and Walker, E.L. (2010). Successful reproduction requires the function of *Arabidopsis* Yellow Stripe-Like1 and Yellow Stripe-Like3 metal-nicotianamine transporters in both vegetative and reproductive structures. Plant Physiol. **154:** 197–210.

Cleaver, O.B., Patterson, K.D., and Krieg, P.A. (1996). Overexpression of the tinman-related genes XNkx-2.5 and XNkx-2.3 in *Xenopus* embryos results in myocardial hyperplasia. Development **122:** 3549–3556.

Clough, S.J., and Bent, A.F. (1998). Floral dip: a simplified method for *Agrobacterium*-mediated transformation of *Arabidopsis thaliana.* Plant J. **16:** 735–743.

Connolly, E.L., Fett, J.P., and Guerinot, M.L. (2002). Expression of the IRT1 metal transporter is controlled by metals at the levels of transcript and protein accumulation. Plant Cell **14:** 1347–1357.

Curie, C., Cassin, G., Couch, D., Divol, F., Higuchi, K., Le Jean, M., Misson, J., Schikora, A., Czernic, P., and Mari, S. (2009). Metal movement within the plant: contribution of nicotianamine and yellow stripe 1-like transporters. Ann. Bot. (Lond.) **103:** 1–11.

DiDonato, R.J., Jr., Roberts, L.A., Sanderson, T., Eisley, R.B., and Walker, E.L. (2004). *Arabidopsis* Yellow Stripe-Like2 (YSL2): a metal-regulated gene encoding a plasma membrane transporter of nicotianamine-metal complexes. Plant J. **39:** 403–414.

Dix, D.R., Bridgham, J.T., Broderius, M.A., Byersdorfer, C.A., and Eide, D.J. (1994). The FET4 gene encodes the low affinity Fe(II) transport protein of *Saccharomyces cerevisiae.* J. Biol. Chem. **269:** 26092–26099.

Durrett, T.P., Gassmann, W., and Rogers, E.E. (2007). The FRD3-mediated efflux of citrate into the root vasculature is necessary for efficient iron translocation. Plant Physiol. **144:** 197–205.

Eide, D., Broderius, M., Fett, J., and Guerinot, M.L. (1996). A novel iron-regulated metal transporter from plants identified by functional expression in yeast. Proc. Natl. Acad. Sci. USA **93:** 5624–5628.

García, M.J., Romera, F.J., Stacey, M.G., Stacey, G., Villar, E., Alcántara, E., and Pérez-Vicente, R. (2013). Shoot to root communication is necessary to control the expression of iron-acquisition genes in Strategy I plants. Planta **237:** 65–75.

Gayomba, S.R., Jung, H.I., Yan, J., Danku, J., Rutzke, M.A., Bernal, M., Krämer, U., Kochian, L.V., Salt, D.E., and Vatamaniuk, O.K. (2013). The CTR/COPT-dependent copper uptake and SPL7-dependent copper deficiency responses are required for basal cadmium tolerance in *A. thaliana.* Metallomics **5:** 1262–1275.

Green, L.S., and Rogers, E.E. (2004). FRD3 controls iron localization in *Arabidopsis.* Plant Physiol. **136:** 2523–2531.

Grusak, M.A., and Pezeshgi, S. (1996). Shoot-to-root signal transmission regulates root Fe(III) reductase activity in the *dgl* mutant of pea. Plant Physiol. **110:** 329–334.

Grusak, M.A., Welch, R.M., and Kochian, L.V. (1990). Physiological characterization of a single-gene mutant of *Pisum sativum* exhibiting excess iron accumulation: I. Root iron reduction and iron uptake. Plant Physiol. **93:** 976–981.

Hasan, S.A., Fariduddin, Q., Ali, B., Hayat, S., and Ahmad, A. (2009). Cadmium: toxicity and tolerance in plants. J. Environ. Biol. **30:** 165–174.

Hindt, M.N., and Guerinot, M.L. (2012). Getting a sense for signals: Regulation of the plant iron deficiency response. Biochim. Biophys. Acta **1823:** 1521–1530.

Ishimaru, Y., Masuda, H., Bashir, K., Inoue, H., Tsukamoto, T., Takahashi, M., Nakanishi, H., Aoki, N., Hirose, T., Ohsugi, R., and Nishizawa, N.K. (2010). Rice metal-nicotianamine transporter, OsYSL2, is required for the long-distance transport of iron and manganese. Plant J. **62:** 379–390.

Järup, L. (2003). Hazards of heavy metal contamination. Br. Med. Bull. **68:** 167–182.

Jefferson, R.A., Kavanagh, T.A., and Bevan, M.W. (1987). GUS fusions: beta-glucuronidase as a sensitive and versatile gene fusion marker in higher plants. EMBO J. **6:** 3901–3907.

Jung, H.I., Gayomba, S.R., Rutzke, M.A., Craft, E., Kochian, L.V., and Vatamaniuk, O.K. (2012). COPT6 is a plasma membrane transporter that functions in copper homeostasis in *Arabidopsis* and is a novel target of SQUAMOSA promoter-binding protein-like 7. J. Biol. Chem. **287:** 33252–33267.

Kneen, B.E., Larue, T.A., Welch, R.M., and Weeden, N.F. (1990). Pleiotropic effects of brz: a mutation in *Pisum sativum* (L.) *cv*; Sparkle' conditioning decreased nodulation and increased iron uptake and leaf necrosis. Plant Physiol. **93:** 717–722.

Kobayashi, T., and Nishizawa, N.K. (2012). Iron uptake, translocation, and regulation in higher plants. Annu. Rev. Plant Biol. **63:** 131–152.

Korenkov, V., Hirschi, K., Crutchfield, J.D., and Wagner, G.J. (2007). Enhancing tonoplast Cd/H antiport activity increases Cd, Zn, and Mn tolerance, and impacts root/shoot Cd partitioning in *Nicotiana tabacum* L. Planta **226:** 1379–1387.

Kuruma, A., Hirayama, Y., and Hartzell, H.C. (2000). A hyperpolarization- and acid-activated nonselective cation current in Xenopus oocytes. Am. J. Physiol. Cell Physiol. **279:** 1401–1413.

Lahner, B., Gong, J., Mahmoudian, M., Smith, E.L., Abid, K.B., Rogers, E.E., Guerinot, M.L., Harper, J.F., Ward, J.M., McIntyre, L., Schroeder, J.I., and Salt, D.E. (2003). Genomic scale profiling of nutrient and trace elements in *Arabidopsis thaliana.* Nat. Biotechnol. **21:** 1215–1221.

Li, Z.S., Lu, Y.P., Zhen, R.G., Szczypka, M., Thiele, D.J., and Rea, P.A. (1997). A new pathway for vacuolar cadmium sequestration in *Saccharomyces cerevisiae*: YCF1-catalyzed transport of bis(glutathionato) cadmium. Proc. Natl. Acad. Sci. USA **94:** 42–47.

Lubkowitz, M. (2011). The oligopeptide transporters: a small gene family with a diverse group of substrates and functions? Mol. Plant **4:** 407–415.

Maas, F.M., van de Wetering, D.A., van Beusichem, M.L., and Bienfait, H.F. (1988). Characterization of Phloem iron and its possible role in the regulation of fe-efficiency reactions. Plant Physiol. **87:** 167–171.

Marschner, H. (1995). Mineral Nutrition of Higher Plants. (London; San Diego: Academic Press).

Morrissey, J., Baxter, I.R., Lee, J., Li, L., Lahner, B., Grotz, N., Kaplan, J., Salt, D.E., and Guerinot, M.L. (2009). The ferroportin metal efflux proteins function in iron and cobalt homeostasis in *Arabidopsis.* Plant Cell **21:** 3326–3338.

Mustroph, A., Zanetti, M.E., Jang, C.J., Holtan, H.E., Repetti, P.P., Galbraith, D.W., Girke, T., and Bailey-Serres, J. (2009). Profiling translatomes of discrete cell populations resolves altered cellular priorities during hypoxia in *Arabidopsis.* Proc. Natl. Acad. Sci. USA **106:** 18843–18848.

Nakagawa, T., et al. (2007). Improved Gateway binary vectors: high-performance vectors for creation of fusion constructs in transgenic analysis of plants. Biosci. Biotechnol. Biochem. **71:** 2095–2100.

Nelson, B.K., Cai, X., and Nebenführ, A. (2007). A multicolored set of in vivo organelle markers for co-localization studies in Arabidopsis and other plants. Plant J. **51:** 1126–1136.

Osawa, H., Stacey, G., and Gassmann, W. (2006). ScOPT1 and AtOPT4 function as proton-coupled oligopeptide transporters with broad but distinct substrate specificities. Biochem. J. **393:** 267–275.

Park, J., Song, W.-Y., Ko, D., Eom, Y., Hansen, T.H., Schiller, M., Lee, T.G., Martinoia, E., and Lee, Y. (2012). The phytochelatin transporters AtABCC1 and AtABCC2 mediate tolerance to cadmium and mercury. Plant J. **69:** 278–288.

Pfaffl, M.W., Horgan, G.W., and Dempfle, L. (2002. Relative expression software tool (REST) for group-wise comparison and statistical analysis of relative expression results in real-time PCR. Nucleic Acids Res. **30:** e36.

Piñeros, M.A., Cançado, G.M., and Kochian, L.V. (2008). Novel properties of the wheat aluminum tolerance organic acid transporter (TaALMT1) revealed by electrophysiological characterization in *Xenopus* oocytes: functional and structural implications. Plant Physiol. **147:** 2131–2146.

Rea, P.A. (2012). Phytochelatin synthase: of a protease a peptide polymerase made. Physiol. Plant. **145:** 154–164.

Robinson, N.J., Procter, C.M., Connolly, E.L., and Guerinot, M.L. (1999). A ferric-chelate reductase for iron uptake from soils. Nature **397:** 694–697.

Rogers, E.E., and Guerinot, M.L. (2002). FRD3, a member of the multidrug and toxin efflux family, controls iron deficiency responses in *Arabidopsis.* Plant Cell **14:** 1787–1799.

Roschzttardtz, H., Séguéla-Arnaud, M., Briat, J.-F., Vert, G., and Curie, C. (2011). The FRD3 citrate effluxer promotes iron nutrition between symplastically disconnected tissues throughout *Arabidopsis* development. Plant Cell **23:** 2725–2737.

Rus, A., Baxter, I., Muthukumar, B., Gustin, J., Lahner, B., Yakubova, E., and Salt, D.E. (2006). Natural variants of AtHKT1 enhance Na^+ accumulation in two wild populations of Arabidopsis. PLoS Genet. **2:** 1964–1973.

Salt, D.E., Prince, R.C., Pickering, I.J., and Raskin, I. (1995). Mechanisms of cadmium mobility and accumulation in indian mustard. Plant Physiol. **109:** 1427–1433.

Santi, S., and Schmidt, W. (2009). Dissecting iron deficiency-induced proton extrusion in *Arabidopsis* roots. New Phytol. **183:** 1072–1084.

Schaaf, G., Honsbein, A., Meda, A.R., Kirchner, S., Wipf, D., and von Wirén, N. (2006). AtIREG2 encodes a tonoplast transport protein involved in iron-dependent nickel detoxification in *Arabidopsis thaliana* roots. J. Biol. Chem. **281:** 25532–25540.

Schaaf, G., Schikora, A., Häberle, J., Vert, G., Ludewig, U., Briat, J.F., Curie, C., and von Wirén, N. (2005). A putative function for the *Arabidopsis* Fe-Phytosiderophore transporter homolog AtYSL2 in Fe and Zn homeostasis. Plant Cell Physiol. **46:** 762–774.

Scholz, G., Schlesier, G., and Seifert, K. (1985). Effect of nicotianamine on iron uptake by the tomato mutant chloronerva. Physiol. Plant. **63:** 99–104.

Schuler, M., Rellán-Álvarez, R., Fink-Straube, C., Abadía, J., and Bauer, P. (2012). Nicotianamine functions in the phloem-based transport of iron to sink organs, in pollen development and pollen tube growth in *Arabidopsis.* Plant Cell **24:** 2380–2400.

Shaff, J.E., Schultz, B.A., Craft, E.J., Clark, R.T., and Kochian, L.V. (2010). GEOCHEM-EZ: a chemical speciation program with greater power and flexibility. Plant Soil **330:** 207–214.

Stacey, M.G., Koh, S., Becker, J., and Stacey, G. (2002). AtOPT3, a member of the oligopeptide transporter family, is essential for embryo development in *Arabidopsis.* Plant Cell **14:** 2799–2811.

Stacey, M.G., Osawa, H., Patel, A., Gassmann, W., and Stacey, G. (2006). Expression analyses of *Arabidopsis* oligopeptide transporters during seed germination, vegetative growth and reproduction. Planta **223:** 291–305.

Stacey, M.G., Patel, A., McClain, W.E., Mathieu, M., Remley, M., Rogers, E.E., Gassmann, W., Blevins, D.G., and Stacey, G. (2008). The *Arabidopsis* AtOPT3 protein functions in metal homeostasis and movement of iron to developing seeds. Plant Physiol. **146:** 589–601.

Sunarpi, Y., et al. (2005). Enhanced salt tolerance mediated by AtHKT1 transporter-induced Na unloading from xylem vessels to xylem parenchyma cells. Plant J. **44:** 928–938.

Turgeon, R., and Webb, J.A. (1973). Leaf development and phloem transport in *Cucurbita pepo*: Transition from import to export. Planta **113:** 179–191.

Valko, M., Morris, H., and Cronin, M.T. (2005). Metals, toxicity and oxidative stress. Curr. Med. Chem. **12:** 1161–1208.

Vert, G.A., Briat, J.-F., and Curie, C. (2003). Dual regulation of the *Arabidopsis* high-affinity root iron uptake system by local and long-distance signals. Plant Physiol. **132:** 796–804.

Waters, B.M., Chu, H.-H., Didonato, R.J., Roberts, L.A., Eisley, R.B., Lahner, B., Salt, D.E., and Walker, E.L. (2006). Mutations in *Arabidopsis* yellow stripe-like1 and yellow stripe-like3 reveal their roles in metal ion homeostasis and loading of metal ions in seeds. Plant Physiol. **141:** 1446–1458.

Wintz, H., Fox, T., Wu, Y.Y., Feng, V., Chen, W., Chang, H.S., Zhu, T., and Vulpe, C. (2003). Expression profiles of *Arabidopsis thaliana* in mineral deficiencies reveal novel transporters involved in metal homeostasis. J. Biol. Chem. **278:** 47644–47653.

Wong, C.K., and Cobbett, C.S. (2009). HMA P-type ATPases are the major mechanism for root-to-shoot Cd translocation in *Arabidopsis thaliana.* New Phytol. **181:** 71–78.

Wu, H., Chen, C., Du, J., Liu, H., Cui, Y., Zhang, Y., He, Y., Wang, Y., Chu, C., Feng, Z., Li, J., and Ling, H.Q. (2012). Co-overexpression FIT with AtbHLH38 or AtbHLH39 in *Arabidopsis*-enhanced cadmium tolerance *via* increased cadmium sequestration in roots and improved iron homeostasis of shoots. Plant Physiol. **158:** 790–800.

Xiao, Y.L., Redman, J.C., Monaghan, E.L., Zhuang, J., Underwood, B.A., Moskal, W.A., Wang, W., Wu, H.C., and Town, C.D. (2010). High throughput generation of promoter reporter (GFP) transgenic lines of low expressing genes in *Arabidopsis* and analysis of their expression patterns. Plant Methods **6:** 18.

Zhai, Z., Sooksa-nguan, T., and Vatamaniuk, O.K. (2009). Establishing RNA interference as a reverse-genetic approach for gene functional analysis in protoplasts. Plant Physiol. **149:** 642–652.

Zhang, M.-Y., Bourbouloux, A., Cagnac, O., Srikanth, C.V., Rentsch, D., Bachhawat, A.K., and Delrot, S. (2004). A novel family of transporters mediating the transport of glutathione derivatives in plants. Plant Physiol. **134:** 482–491.